Research Article

Dynamics and Composition of Small Heat Shock Protein Condensates and Aggregates

Joep Joosten [1,2,3*], Bob van Sluijs [2], Wilma Vree Egberts [1], Martin Emmaneel [1], Pascal W. T. C. Jansen [4], Michiel Vermeulen [4], Wilbert Boelens [1†], Kimberly M. Bonger [3†] and Evan Spruijt [2†]

*1 - **Biomolecular Chemistry,** Radboud University Institute for Molecular and Materials, Nijmegen, the Netherlands*
*2 - **Physical Organic Chemistry,** Radboud University Institute for Molecular and Materials, Nijmegen, the Netherlands*
*3 - **Synthetic Organic Chemistry,** Radboud University Institute for Molecular and Materials, the Netherlands*
*4 - **Molecular Biology,** Radboud University Institute for Molecular Life Sciences, Nijmegen, the Netherlands*

Correspondence to Joep Joosten: *Synthetic Organic Chemistry, Radboud University Institute for Molecular and Materials, Nijmegen, the Netherlands. joep.joosten@ru.nl (J. Joosten) @Joosten_J (J. Joosten), @LabVermeulen (M. Vermeulen), @kimbonger (K.M. Bonger), @SpruijtLab (E. Spruijt)*
https://doi.org/10.1016/j.jmb.2023.168139
Edited by J. Buchner

Abstract

Small heat shock proteins (sHSPs) are essential ATP-independent chaperones that protect the cellular proteome. These proteins assemble into polydisperse oligomeric structures, the composition of which dramatically affects their chaperone activity. The biomolecular consequences of variations in sHSP ratios, especially inside living cells, remain elusive. Here, we study the consequences of altering the relative expression levels of HspB2 and HspB3 in HEK293T cells. These chaperones are partners in a hetero-oligomeric complex, and genetic mutations that abolish their mutual interaction are associated with myopathic disorders. HspB2 displays three distinct phenotypes when co-expressed with HspB3 at varying ratios. Expression of HspB2 alone leads to formation of liquid nuclear condensates, while shifting the stoichiometry towards HspB3 resulted in the formation of large solid-like aggregates. Only cells co-expressing HspB2 with a limited amount of HspB3 formed fully soluble complexes that were distributed homogeneously throughout the nucleus. Strikingly, both condensates and aggregates were reversible, as shifting the HspB2:HspB3 balance in situ resulted in dissolution of these structures. To uncover the molecular composition of HspB2 condensates and aggregates, we used APEX-mediated proximity labelling. Most proteins interact transiently with the condensates and were neither enriched nor depleted in these cells. In contrast, we found that HspB2:HspB3 aggregates sequestered several disordered proteins and autophagy factors, suggesting that the cell is actively attempting to clear these aggregates. This study presents a striking example of how changes in the relative expression levels of interacting proteins affects their phase behavior. Our approach could be applied to study the role of protein stoichiometry and the influence of client binding on phase behavior in other biomolecular condensates and aggregates.

Introduction

Small heat shock proteins (sHSPs) are ATP-independent molecular chaperones that are part of the cellular protein quality control system which defends the integrity of the proteome.[1] sHSPs have the ability to bind a large variety of non-native and misfolded proteins, thereby delaying the formation

of irreversible protein aggregates.[2] After being bound by sHSPs, misfolded proteins are either degraded by the proteasome or autophagosomes, or refolded by ATP-dependent chaperones, such as HSP70.[3–7] As misfolding and aberrant aggregation of proteins are central to the etiology of numerous degenerative diseases[8], it is not surprising that mutations in sHSP genes have been linked to various pathological conditions.[9]

The human genome encodes ten sHSPs (HspB1-HspB10), which strongly vary in their tissue expression pattern and levels (Figure S1(A-B)). Four sHSPs (HspB1, HspB5, HspB6, and HspB8) are ubiquitously expressed at relatively high levels,[10] while others are predominantly expressed in specific tissues (Figure S1(A-D)). For instance, HspB2 (also known as MKBP) and HspB3 (also known as HspL27) are upregulated during myoblast differentiation[11] and highly expressed in heart and skeletal muscle (Figure S1(C)).[11–13] All sHSPs contain a highly conserved α-crystallin domain (ACD) at their core, which is responsible for the formation of dimers that may ultimately assemble into polydisperse oligomeric complexes up to 1000 kDa in size.[14] The ACD is flanked by less conserved, flexible N- and C-terminal regions, which are important for the stabilization of these oligomeric complexes,[15–16] and may also mediate phase separation.[17]

A recent study has shown that, in differentiating myoblasts, HspB2 forms both nuclear foci that do not contain HspB3, as well as cytoplasmic foci that colocalize with HspB3.[18] These findings indicate that HspB2 and HspB3 can form multimeric assemblies of diverse compositions in vivo. The dynamics, molecular composition and functional significance of these different structures is currently unknown. By contrast, it has been shown that HspB2 and HspB3 form a stable hetero-tetrameric complex with a well-defined 3:1 ratio in vitro.[19,20] While it remains unclear if these chaperones interact in the same way in living cells, it is likely that their balanced expression is important for their subcellular distribution and chaperone activity.[21] The importance of a tightly regulated HspB2:HspB3 balance is underscored by the fact that a mutation in HspB3 which disrupts the interaction between the two proteins results in aberrant HspB2 phase separation that ultimately leads to myopathy.[18] Thus far, the effects of variation in relative HspB2:HspB3 expression levels on complex formation and distribution inside livings cells remain enigmatic.[18] Identification of potential sequestered proteins and additional interactors may help uncover the role of small heat shock protein foci, thereby further elucidating their function and involvement in the development of degenerative diseases.

Here, we show that HspB2 forms nuclear foci through liquid–liquid phase separation in the absence of HspB3. Co-expression of a limited amount of HspB3 resulted in dissolution of HspB2 condensates and homogeneous distribution of HspB2 in the nucleus, while further shifting the balance towards HspB3 resulted in the formation of nuclear and cytoplasmic aggregates. The cytoplasmic aggregates in particular can be very large and dramatically impact nuclear morphology. To elucidate the composition of HspB2 condensates and HspB2:HspB3 aggregates, we used proximity labeling mediated by the engineered peroxidase APEX.[22] We found that HspB2:HspB3 aggregates were highly enriched for core autophagy factors, such as SQSTM1 (also known as p62), suggesting that these aggregates are targeted by the autophagosome. In contrast, very few proteins were strongly enriched or depleted in nuclear HspB2 condensates, suggesting that most proteins are able to transiently shuttle in and out of the condensates.

Results

HspB2 forms condensates through liquid–liquid phase separation

As a member of the sHSP family,[16] HspB2 contains the characteristic α-crystallin domain (ACD) domain, flanked by less structurally defined N- and C- terminal tails (Figure 1(A)). Moreover, the C-terminal tail is highly enriched in negatively charged amino acids, including a repeat of five glutamic acid (E) residues (Figure 1(A)). In recent years, it has become evident that disordered regions in proteins can serve important biological functions[23–24] and may mediate the formation of condensates through liquid–liquid phase separation.[25] Indeed, it has been shown that HspB2 phase separates into nuclear condensates in differentiating myoblasts.[18] However, what is not yet clear is how variations in relative expression levels of sHSPs, such as HspB2 and HspB3, can alter their phase behavior.

Here, we used HEK293T cells to study the effects of altering the relative HspB2:HspB3 expression levels, as these cells do not express HspB2 and HspB3 endogenously. We found that HspB2 forms nuclear foci when overexpressed in HEK293T cells (Figure 1(B)). To assess the contribution of the disordered N- and C- termini to the formation of these nuclear HspB2 foci, we generated truncation mutants lacking these tails (schematically shown in Figure 1(A)). While removal of the N-terminus (ΔN) did not affect HspB2 localization, removal of the negatively charged C-terminal tail (ΔC) abolished the formation of nuclear foci, and resulted in a diffuse nuclear distribution of the truncated HspB2 protein (Figure 1(B)), similar to what was observed previously in differentiating myoblasts.[18]

The circularity of the nuclear foci implies a liquid state, suggesting that liquid–liquid phase separation may underlie their formation. To prove the liquid nature of these foci, we performed live

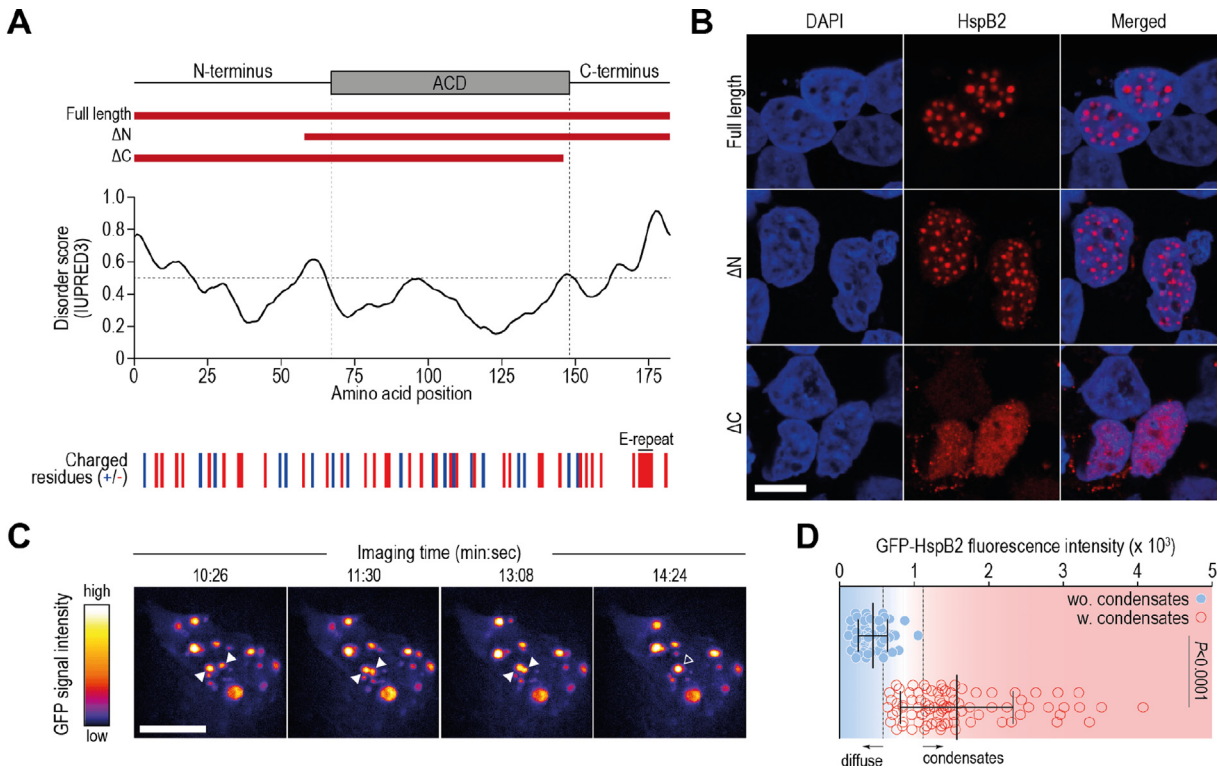

Figure 1. HspB2 phase separation into nuclear liquid droplets is regulated by its disordered C-terminus (A) Schematic representation of the HspB2 protein, with the α-crystallin domain (ACD) indicated in grey. Indicated below are the truncation mutants ΔN and ΔC used in (B). The disorder score was determined using IUPRED3. On the bottom, the position of positively (blue; lysine, arginine, and histidine) and negatively (red; aspartic acids and glutamic acid) charged amino acid residues is indicated. **(B)** Confocal microscopy images of HEK293T cells expressing the transgenic constructs depicted in (A), stained using an antibody against HspB2. The scalebar represents 10 μm. **(C)** Screenshots taken from a video of a HEK293T cell expressing (GFP)-HspB2. Imaging started ∼ 16 hours after transfection and continued for ∼15 minutes with an image being taken every 2 seconds. Droplets that will undergo fusion are indicated by closed arrowheads, the fused droplet is indicated by an open arrowhead. The scalebar represents 10 μm. **(D)** Average GFP-HspB2 fluorescence intensity distribution of cells transfected with GFP-HspB2 and untagged HspB2 at a 1:8 ratio. The diffuse (non-condensate) GFP-HspB2 signal was quantified in cells in which condensates were formed (red) and in cells lacking observable condensates (blue). Line and whiskers indicate the mean and standard deviation. A Kolmogorov-Smirnov non-parametric test was performed to determine statistical significance. See also Figure S2 and Videos S1-3.

imaging and fluorescence recovery after photobleaching (FRAP) of HEK293T cells expressing HspB2 and GFP-tagged HspB2 at a 1:8 ratio. At this ratio, the GFP-HspB2 signal recapitulated the nuclear foci previously observed for untagged HspB2 alone (Figure S2(A)). During live imaging, we predominantly observed dynamically moving nuclear droplets (Video S1), which fuse upon collision (Figure 1(C) and Video S2), proving their liquid nature. As liquid–liquid phase separation is known to occur above a threshold protein concentration,[25] we quantified the average fluorescence intensity of the diffuse (non-condensate) signal in cells containing HspB2 condensates and in cells lacking condensates. We found that condensates indeed form above a defined threshold concentration (Figure 1(D)), further supporting that liquid–liquid phase separation underlies their formation. Finally, we found that the fluorescence signal recovers quickly after partial photobleaching of a condensate (Figure S2(B), Video S3A), indicating fast protein diffusion within the droplet. Together, these data show that HspB2 forms nuclear droplets through liquid–liquid phase separation, and that the disordered C-terminus is required for this phase separation.

Co-expression of HspB3 disrupts the formation of HspB2 condensates

As HspB2 directly interacts with HspB3,[18–20] we next assessed the effect of HspB3 co-expression on the subcellular localization and phase behavior of HspB2. We first determined how the ratio of transfected HspB2:HspB3 plasmid DNA correlates to the amount of protein produced (Figure S3(A-D) and accompanying legend). While this correlation

was not linear, the amount of transfected plasmid DNA strongly correlated with the amount of protein produced. We then investigated which phenotypes emerged from co-expressing HspB2 and HspB3 at different ratios. While HspB2 localized to nuclear condensates in the absence of HspB3, co-expression of a small amount of HspB3 resulted in a diffuse nuclear distribution of HspB2, reminiscent of the stable and soluble HspB2-HspB3 oligomers that were reported in vitro (Figure 2(A)). Interestingly however, we observed that co-expression of a larger amount of HspB3 resulted in the localization of HspB2 to amorphous structures, both in the nucleus and in the cytoplasm. Although it is not known if these structures contain irretrievably damaged proteins (and as such can be considered 'real' aggregates[26]) or whether the proteins contained within retain some of their biological function, we opted to use the term "aggregate" to refer to these amorphous HspB2:HspB3 structures throughout the manuscript.

While nuclear HspB2 condensates are dynamically moving circular droplets, HspB2:HspB3 aggregates are much more static (Video S4), irregularly shaped (Figure 2(C-D)) and do not recover after photobleaching (Figure S2(B), Video S3B-C), suggesting a more solid-like composition. Both the small HspB2 condensates, as well as the nuclear HspB2:HspB3 aggregates displaced chromatin (Figure 2(B)), potentially affecting gene expression and other nuclear processes. Nonetheless, we did not observe obvious

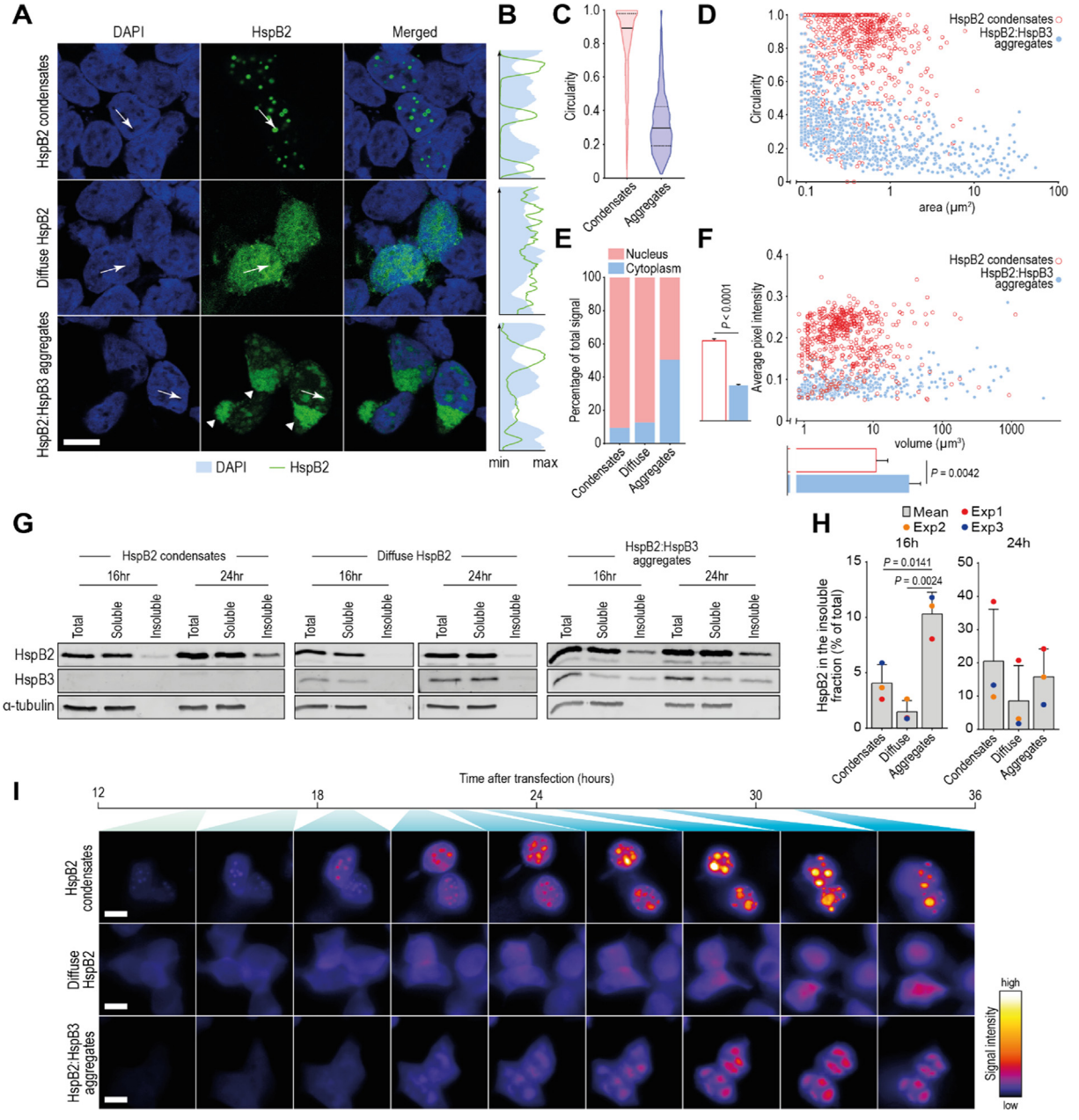

detrimental effects on cell survival or proliferation for any of the HspB2:HspB3 expression ratios used (Figure S3(E)).

To verify that some aggregates at high HspB3 levels are indeed cytoplasmic, we combined HspB2 imaging with staining of Lamin A and Lamin B1; structural components of the nuclear lamina which line the inner membrane of the nuclear envelope.[27] This experiment showed that these large aggregates are indeed outside the nuclear perimeter (Figure S4(A)), underscoring that HspB2 and HspB3 can aggregate in both nuclear and cytoplasmic aggregates. Remarkably, we found that in cells containing HspB2 condensates, a fraction of the Lamin B1 colocalized with HspB2 (Figure S4(A-B)). In these cells, Lamin B1 still showed a continuous lining of the nuclear envelope, suggesting that the integrity of the envelope was not compromised by this sequestration. In contrast with a previous study in myoblasts,[18] we did not observe colocalization of HspB2 with Lamin A (Figure S4(C-D)), suggesting that Lamin A sequestration in HspB2 condensates formed in myoblasts is likely mediated by factors that are not expressed in HEK293T cells.

To measure HspB2 subcellular localization, and to quantify the number, volume, and relative intensities of HspB2 condensates and HspB2:HspB3 aggregates, we performed high-throughput 3D imaging, followed by automated image analysis (see Figure S5 and accompanying Supplemental text for validation of the method). First, we assessed subcellular localization globally by determining the relative amount of HspB2-signal in the nucleus and the cytoplasm. This analysis revealed that in cells containing HspB2 condensates, the vast majority (91%) of HspB2 resides within the nucleus (Figure 2(E)). In cells containing HspB2:HspB3 aggregates, HspB2 was distributed equally over both the nucleus (49%) and cytoplasm (51% - Figure 2(E)). We then compared the volume of HspB2 condensates and HspB2:HspB3 aggregates, as well as the average HspB2 signal intensity in both structures. While HspB2 condensates were on average smaller than HspB2:HspB3 aggregates (11.5 μm^3 vs. 34.6 μm^3, respectively - Figure 2(F)), their fluorescence intensity was higher, indicating that the HspB2 concentration is higher in HspB2 condensates than in HspB2:HspB3 aggregates (Figure 2(F)). Taken together, these results show that HspB2 condensates and HspB2:HspB3 aggregates are different subcellular structures with distinct physical and chemical properties.

It has been shown previously that a myopathy-associated mutation in the HspB3 gene (HspB3-R116P) prevents HspB3 from interacting with HspB2.[18] We used this mutant to assess whether a direct interaction between HspB2 and HspB3 is required for the formation of HspB2:HspB3 aggregates. As in previous experiments (Figure 2(A)), co-transfection of a high amount of wild-type (WT) HspB3 caused colocalization of both proteins in amorphous aggregates (Figure S3(F-G)). Replacing HspB3-WT with HspB3-R116P resulted in the formation of HspB2 condensates and distinct

Figure 2. Relative HspB2:HspB3 levels determine the formation of liquid HspB2 condensates and solid-like HspB2:HspB3 aggregates (A) Confocal images of HEK293T cells containing HspB2 condensates, diffuse nuclear HspB2, or HspB2:HspB3 aggregates. GFP-tagged HspB2 was co-expressed at a 1:8 ratio with untagged HspB2 to visualize the protein directly (also for (I)). The scalebar represents 10 μm, arrowheads indicate cytoplasmic aggregates and the arrows designate the direction along which the histograms shown in (B) were determined. **(B)** Histograms depicting HspB2 and DAPI signal intensities along the lines shown in (A). **(C)** Violin plots showing the circularity of HspB2 condensates and HspB2:HspB3 aggregates. **(D)** Scatter plot depicting the area (x-axis) and circularity (y-axis) of HspB2 condensates and HspB2:HspB3 aggregates. **(E)** The percentage of pixels located in the nucleus and cytoplasm in HEK293T cells containing HspB2 condensates, diffuse HspB2 staining, and HspB2:HspB3 aggregates. **(F)** Scatter plot depicting the volume (x-axis) and average pixel intensities (y-axis) for in HspB2 condensates and HspB2:HspB3 aggregates. Bars and whiskers represent the mean and 95% confidence interval, non-parametric Kolmogorov-Smirnov tests were used to determine statistical significance. The width of the bars is proportional to the number of HspB2-foci identified in each dataset. **(G)** Western blot analysis depicting the solubility of HspB2 and HspB3 in lysates from HEK293T cells with indicated HspB2 subcellular distribution phenotypes. Cells were lysed 16 and 24 hours after transfection and fractionated into total, soluble (supernatant) and insoluble (pellet) fractions by centrifugation. **(H)** Quantification of three replicate western blotting experiments (See supplemental dataset 1). The HspB2 signals were quantified, normalized to the α-tubulin signal in the total lysate sample from the corresponding transfection, and expressed as a percentage of total HspB2. Bars and whiskers are the mean and standard deviation of three biological replicates, colored dots indicate the values from individual experiments. The western blot in (G) is from experiment #3, see also Supplemental Dataset 1 for the raw data underlying this bar graph. Student's t-tests with correction for multiple testing using the Holm-Šídák method was performed to determine statistical significance. **(I)** Screen shots from videos of HEK293T cells developing HspB2 condensates, diffuse nuclear HspB2 signal, and HspB2:HspB3 aggregates. Imaging started approximately 12 hours after transfection, with an image being taken every 15 minutes for 24 hours. Blue shading corresponds to the position in the timeline shown above. All scalebars represent 10 μm. See also Figures S2-5 and Videos S4-5.

nuclear foci containing HspB3-R116P (Figure S(G-H)), as observed previously.[28] These findings indicate that a direct interaction between HspB2 and HspB3 is required for their colocalization in aggregates and that both proteins can translocate across the nuclear membrane independently, despite lacking canonical nuclear localization sequences. This is underscored by the fact that HspB3-WT also accumulates in nuclear aggregates when expressed without HspB2 (Figure S3(H)).

Separation of the soluble and insoluble fractions of lysates prepared from cells expressing HspB2 and HspB3 at various ratios, confirms that the diffusely distributed HspB2 forms mostly soluble complexes (Figure 2(G-H) and Supplemental Dataset 1). In contrast, in cells containing HspB2 condensates or HspB2:HspB3 aggregates, a sizeable fraction of both proteins is present in complexes that are insoluble by detergents.

In several contexts, it has been shown that liquid droplets may transition into more solid-like aggregates.[29–31] To assess whether such gradual solidification of liquid droplets underlies the formation of HspB2:HspB3 aggregates, we investigated the development of HspB2 condensates and HspB2:HspB3 aggregates over time. In the absence of HspB3, HspB2 accumulated in dynamically moving, circular condensates that nucleated in multiple locations and progressively increased in size through growth and coalescence (Figure 2(I) – top row and Video S5A). HspB2 was uniformly distributed throughout the nucleus upon co-expression of a small amount of HspB3 (Figure 2(I) – middle row and Video S5B). When further shifting the HspB2:HspB3 stoichiometry towards HspB3, HspB2 formed amorphous aggregates which became observable approximately 18 hours after transfection, and increased in size over time (Figure 2(I) – bottom row and Video S5C). Importantly, from the moment they became detectable, these structures were not circular, suggesting that they did not form through fusion and gradual solidification of liquid droplets, but rather started out as amorphous aggregates that steadily grew over time. Altogether, these data indicate that tight regulation of the relative expression of HspB2 and HspB3 is highly important for the correct subcellular distribution of these chaperone proteins.

HspB2 condensates and HspB2:HspB3 aggregates are fully reversible

To probe the reversibility of HspB2 condensate and HspB2:HspB3 aggregate formation, we performed a sequential transfection experiment, in which we first triggered the formation of HspB2 condensates and HspB2:HspB3 aggregates, and subsequently performed a second transfection, which shifted the HspB2:HspB3 ratio in situ (Figure 3(A)). It is important to note that we added GFP-tagged HspB2 at a 1:8 ratio with untagged HspB2 only in the second transfection to enable the distinction between cells hit during the first and second transfection. Afterwards, we assessed the effect of shifting the HspB2:HspB3 stoichiometry on HspB2 condensates and aggregates. In cells transfected with HspB2 alone, we readily detected nuclear HspB2 condensates (Figure 3(B) and closed arrowheads in Figure 3(C)). Subsequent transfection with myc-tagged HspB3 led to the formation of HspB3 aggregates in cells that were not hit in the first transfection round (open arrowheads in Figure 3(C)), and amorphous nuclear HspB2:HspB3 aggregates in cells that contained HspB2 from the first transfection (arrow in Figure 3(C)). These findings indicate that addition of HspB3 is able to disrupt pre-formed HspB2 condensates, resulting in the nuclear aggregation of both chaperones.

As before, HspB2:HspB3 protein aggregates were readily formed upon equimolar transfection of plasmids encoding both proteins (Figure 3(D) and closed arrowheads in Figure 3(E)). Intriguingly, shifting the HspB2:HspB3 balance by expressing additional HspB2 in a second transfection resulted in the dissolution of aggregates (arrow in Figure 3(E-F)). These data show that HspB2 condensate and HspB2:HspB3 aggregate formation is reversible, suggesting that the underlying intermolecular interactions are sufficiently weak to allow for dynamic exchange of components.

Proximity labeling of HspB2 condensates and HspB2:HspB3 aggregates

Both condensates and aggregates are expected to interact with, and potentially trap specific sets of proteins, which may be linked to associated pathologies. To elucidate the composition of HspB2 condensates and aggregates, we employed APEX-mediated proximity labelling.[22] In brief, plasmids encoding APEX-tagged transgenes were transfected into HEK293T cells to trigger the formation of HspB2 condensates, diffuse nuclear HspB2 distribution, and HspB2:HspB3 aggregates. As controls, cells expressing APEX fused to a nuclear localization signal (NLS) or nuclear export signal (NES), and cells expressing only untagged HspB2 (no APEX) were used (Figure S6(A)). Upon incubation with biotin-phenol and subsequent treatment with hydrogen peroxide, the APEX enzyme generates short lived biotin-phenoxyl radicals which covalently bind to proximal proteins.[32–33] After labelling, biotinylated proteins were enriched on streptavidin-conjugated beads and digested for identification by mass spectrometry (Figure 4(A)).

We first evaluated the specificity of APEX-proximity labelling by visualizing biotinylation with an fluorophore coupled streptavidin. For all conditions, the biotinylation patterns mirrored those observed previously when using untagged or GFP-tagged HspB2 constructs (Figure 4(B)). As expected, the APEX-NES and APEX-NLS

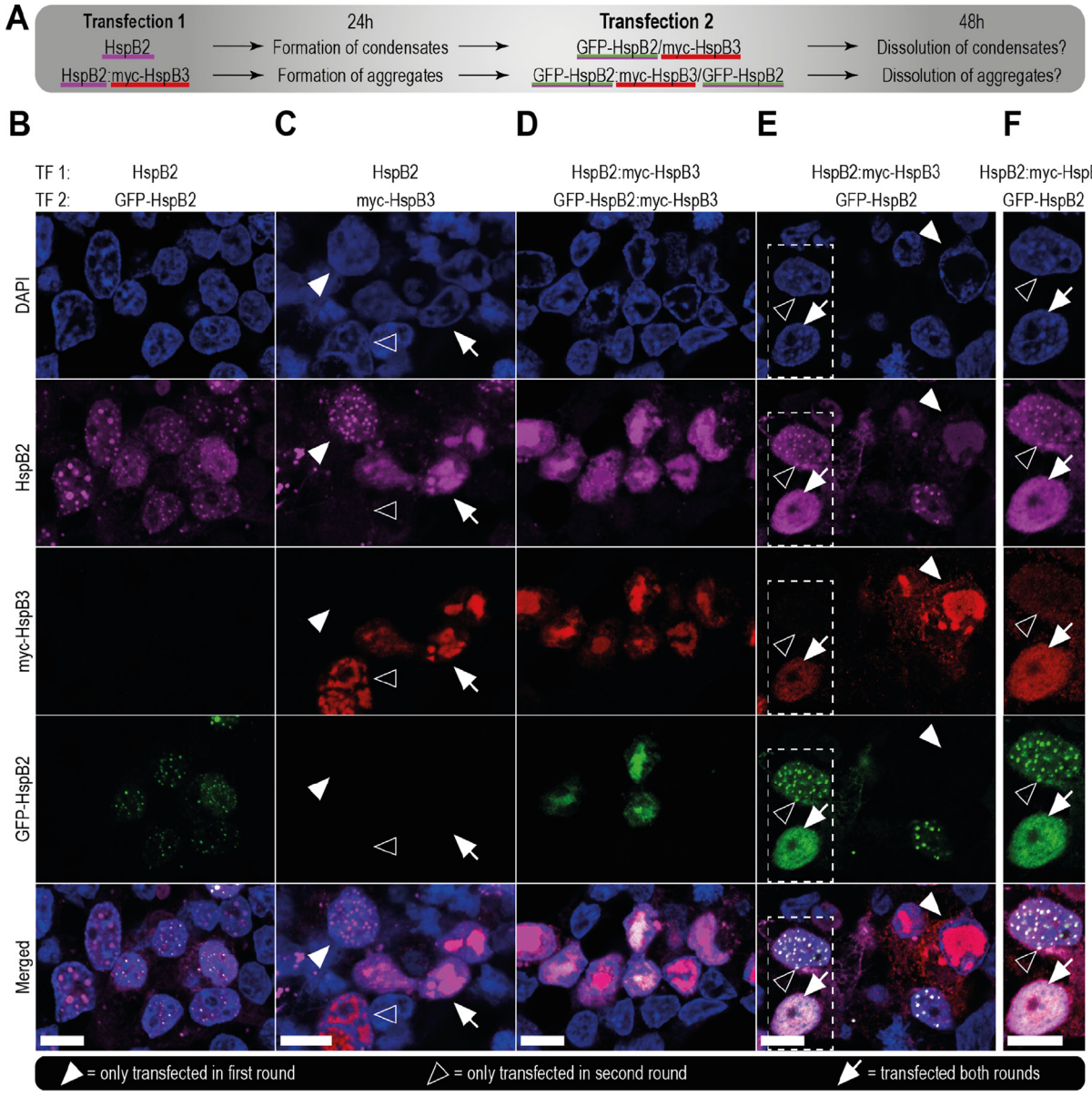

Figure 3. Dissolution of HspB2 condensates and HspB2:HspB3 aggregates by shifting the HspB2:HspB3 ratio in situ(A) Schematic overview of the transfection schemes used in the experiment shown in Figure panels (B-F). The colored underlining corresponds to the colors used for visualization of the various proteins in (B-F). **(B-E)** Confocal images depicting HEK293T cells transfected using the transfection schemes shown in (A). Closed arrowheads indicate cells hit with the first transfection (TF1), but not the second; open arrowheads indicate cells hit only in the second transfection (TF2). Arrows indicate cells that were transfected in both rounds. Antibody staining was used to visualize HspB2 and myc-HspB3, while GFP-tagged HspB2 was used to identify cells hit in the second transfection round in indicated samples. All scalebars are 10 μm (same for (F)). **(F)** Magnification of the area denoted by the dashed box in (E). The myc-HspB3 signal was digitally enhanced to improve the visibility of the weaker diffuse signal.

controls show cytoplasmic and nuclear biotinylation, respectively, while no labelling is observed in cells lacking an APEX-construct (no APEX). We next performed streptavidin enrichment on lysates from cells expressing the various constructs mentioned above, and assessed biotinylation patterns and protein enrichment through western blotting (Figure 4(C) and Figure S6(B)).

Unbound nuclear proteins can freely shuttle between HspB2 condensates and the nucleoplasm

Proteins biotinylated in HspB2 condensates were purified on streptavidin beads, and digested to

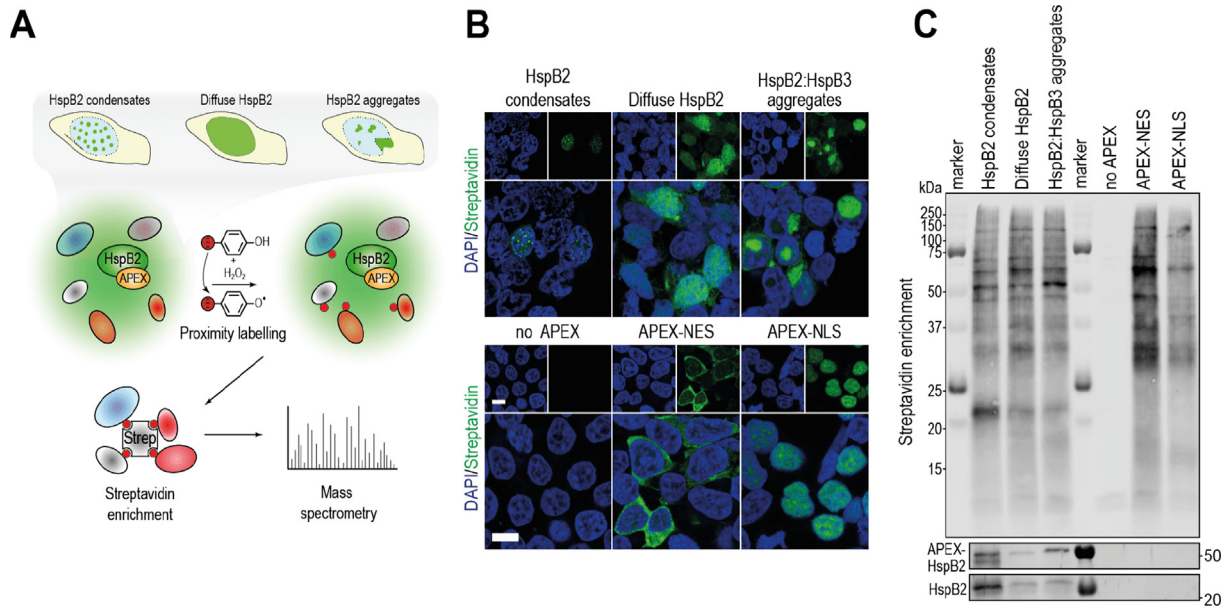

Figure 4. APEX proximity labelling of HspB2 condensates and HspB2:HspB3 aggregates (A) Schematic representation of the APEX proximity labelling approach used to determine the composition of HspB2 condensates and HspB2:HspB3 aggregates. **(B)** Confocal microscopy imaging of APEX-mediated biotinylation in HEK293T cells with indicated HspB2 phenotypes, and in no APEX, APEX-NES and APEX-NLS controls. The scale bars denote 10 μm. An Alexa488-fluorophore coupled Streptavidin was used to visualize biotinylated proteins. **(C)** Streptavidin blotting of enriched proteinsfrom lysates of cells expressing various transgenes. APEX-tagged and untagged HspB2 were detected using an antibody targeting HspB2.

peptides which were measured by mass spectrometry. As these condensates are virtually exclusively nuclear (Figure 2(E)), we calculated enrichments relative to the APEX-NLS control. As expected, HspB2 is dramatically enriched (>26,000-fold; Figure 5(A)), indicating efficient auto-biotinylation. In line with previous studies,[34–35] we found enrichments of HspB1 (22-fold) and BAG3 (6-fold) in HspB2 condensates, indicating that our method is able to identify known interactions. In addition, we uncover previously unknown interactions with various proteins including LGALS7 (~78-fold), and MEA1 (~26-fold). For gene ontology (GO)-term enrichment analysis, we selected the top 5% enriched factors with a *P*-value < 0.01 (blue in Figure 5(A), listed in Table S1A). This analysis uncovered an enrichment of components of the HAUS complex (Figure 5(B)); a complex that localizes to the centrosome during in mitotic spindle assembly. While it has previously been reported that HspB7 associates with nuclear substructures such as PML bodies and SC35 speckles,[36] we do not observe colocalization of HspB2 with markers for these substructures (Figure S7(A)). Moreover, components of these and other nuclear substructures are not enriched in our HspB2 condensate proximity labelling dataset, indicating that HspB2 droplets represent a distinct nuclear substructure.

To analyze the group of proteins that was depleted from HspB2 condensates, we next assessed GO-term enrichment for the top 5% depleted factors with a *P*-value < 0.01 (red in Figure 5(A), listed in Table S1B). Proteins bound to chromatin, histones and DNA are significantly depleted from HspB2 condensates (Figure 5(C)), suggesting that these proteins are unavailable for shuttling into the condensates because of their association with the genome. In line with this, proteins enriched in HspB2 condensates are depleted for the GO-terms chromatin-binding, histone binding and DNA binding (n = 0, n = 0, and n = 2 out of 48 proteins, respectively).

As intrinsic protein disorder is considered to be a major contributing factor in condensate formation,[37] we subsequently compared the amount of disorder in proteins enriched in, and depleted from HspB2 condensates. Proteins enriched in condensates are significantly more disordered compared to the median degree of disorder of nuclear proteins (33.9% vs. 25.1%, respectively; Figure 5(D)). Intriguingly however, proteins that were significantly depleted from condensates displayed an even larger degree of disorder (median disorder 50.2%), which may be explained by the fact that transcription factors and chromatin remodelers generally contain a high degree of disorder.[38–40] Furthermore, nuclear proteins overall display a larger degree of intrinsic disorder (25.2% - Figure S7(B)) than cytoplasmic proteins (11.0%) or proteins that shuttle between nucleus and cytoplasm (17.0%). Aside

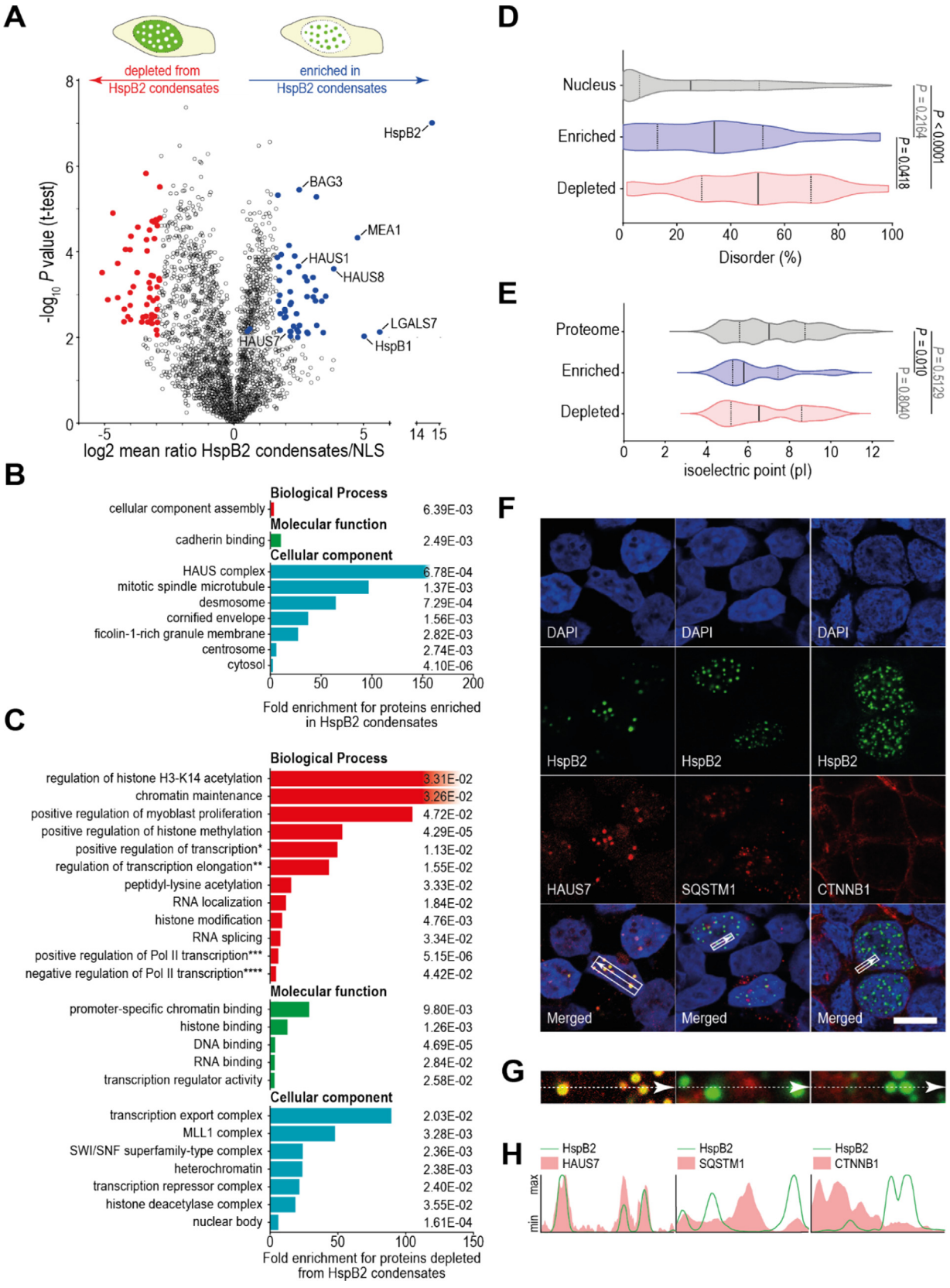
A
depleted from HspB2 condensates
enriched in HspB2 condensates
HspB2
BAG3
MEA1
HAUS1
HAUS8
LGALS7
HspB1
HAUS7
-log10 P value (t-test)
log2 mean ratio HspB2 condensates/NLS
B
Biological Process
cellular component assembly 6.39E-03
Molecular function
cadherin binding 2.49E-03
Cellular component
HAUS complex 6.78E-04
mitotic spindle microtubule 1.37E-03
desmosome 7.29E-04
cornified envelope 1.56E-03
ficolin-1-rich granule membrane 2.82E-03
centrosome 2.74E-03
cytosol 4.10E-06
Fold enrichment for proteins enriched in HspB2 condensates
C
Biological Process
regulation of histone H3-K14 acetylation 3.31E-02
chromatin maintenance 3.26E-02
positive regulation of myoblast proliferation 4.72E-02
positive regulation of histone methylation 4.29E-05
positive regulation of transcription* 1.13E-02
regulation of transcription elongation** 1.55E-02
peptidyl-lysine acetylation 3.33E-02
RNA localization 1.84E-02
histone modification 4.76E-03
RNA splicing 3.34E-02
positive regulation of Pol II transcription*** 5.15E-06
negative regulation of Pol II transcription**** 4.42E-02
Molecular function
promoter-specific chromatin binding 9.80E-03
histone binding 1.26E-03
DNA binding 4.69E-05
RNA binding 2.84E-02
transcription regulator activity 2.58E-02
Cellular component
transcription export complex 2.03E-02
MLL1 complex 3.28E-03
SWI/SNF superfamily-type complex 2.36E-03
heterochromatin 2.38E-03
transcription repressor complex 2.40E-02
histone deacetylase complex 3.55E-02
nuclear body 1.61E-04
Fold enrichment for proteins depleted from HspB2 condensates
D
Nucleus
Enriched
Depleted
P = 0.2164
P = 0.0418
P < 0.0001
Disorder (%)
E
Proteome
Enriched
Depleted
P = 0.010
P = 0.8040
P = 0.5129
isoelectric point (pI)
F
DAPI
HspB2
HAUS7
SQSTM1
CTNNB1
Merged
G
H
HspB2
HAUS7
SQSTM1
CTNNB1
max
min

from its disorder, a proteins charge state may greatly affect its phase behavior.[41] We therefore also evaluated the isoelectric point (pI) of proteins enriched in, and depleted from HspB2 condensates. Proteins enriched in condensates had a significantly lower pI compared to the proteome (Figure 5(E)), suggesting that charge interactions may contribute to the protein uptake into HspB2 condensates.

While it is interesting to identify specific proteins that were enriched or depleted from condensates, perhaps the most striking result from our proximity labeling analysis is the fact that the vast majority of proteins are neither enriched nor depleted. We found that for the comparison of HspB2 condensates vs. APEX-NLS, 97.4% of all identified proteins had log2 enrichment scores between -2.89 (e^{-2}) and 2.89 (e^{2}), corresponding to a partitioning free energy difference of less than 2 k_BT (Figure S7(C)). This suggests that most of the detected nuclear proteins are able to shuttle freely in and out of HspB2 condensates, and have a negligible preference for being inside the condensate over the nucleoplasm, or vice versa. If they would have had a strongly unfavorable interaction with condensate components, they would hardly enter the condensates and we would expect these proteins to be strongly depleted in our proximity labelling dataset. On the other hand, if they would have a strongly favorable interaction with condensate components, they would be unlikely to leave the condensates and we would expect these proteins to be strongly enriched. Our findings suggest that the vast majority of unbound nuclear proteins shuttle freely in and out of condensates, without getting trapped.

To confirm that our proximity labelling of HspB2 condensates is able to identify novel interactors, we performed colocalization imaging using an antibody against the hitherto unknown interactor HAUS7. In line with earlier findings,[42] HAUS7 shows cytoplasmic and nucleolar staining in untransfected cells (Supplemental Dataset 2). In HEK293T cells containing HspB2 condensates, HAUS7 is also recruited to these nuclear foci (Figure 5(F-H)), validating the enrichment observed in our proximity labelling. In agreement with earlier work,[43] SQSTM1 (also known as p62) localized to cytoplasmic and nuclear foci in untransfected cells (Supplemental Dataset 2). These foci do not colocalize with HspB2 condensates (Figure 5(F-H)), which is in line with its lack of enrichment in our proximity labelling dataset. Previous work showed the *O*-GlcNAcylation-dependent translocation of CTNNB1 to the plasma membrane.[44] In line with this, we observe CTNBB1-staining at the cell membrane, which therefore does not overlap with the nuclear HspB2-signal (Figure 5(F-H)). A schematic representation of domain composition, charge distribution and predicted disorder of HAUS7, SQSTM1 and CTNNB1 is shown in Figure S7(D).

HspB2:HspB3 aggregates sequester disordered proteins and autophagy factors

We next set out to elucidate the composition of the amorphous HspB2:HspB3 aggregates. As these aggregates are equally present in the nucleus and cytoplasm (Figure 2(E)), we calculated enrichments relative to both APEX-NES and APEX-NLS controls. HspB2 and HspB3 were strongly enriched (13,000-fold (vs. NES)/22,000-fold (vs. NLS) and 12,000-fold (vs. NES)/15,000-fold (vs. NLS), respectively), indicating a very strong interaction between the two chaperone proteins (Figure 6(A-B)). As seen for HspB2 condensates, known interactors BAG3 (11-fold (vs. NES)/23-fold (vs. NLS)) and HspB1

Figure 5. Unbound nuclear proteins freely shuttle between nucleoplasm and HspB2 condensates (A) Volcano plot depicting the mean ratio of proximal proteins detected upon APEX-labelling in HspB2 condensates vs. cells expressing APEX-NLS. The top 5% proteins enriched in HspB2 condensates are depicted in blue, red circles indicate the 5% proteins most depleted from HspB2 condensates. **(B)** GO-term enrichment analysis for factors enriched in HspB2 condensates (blue in (A)), as determined using gene ontology analysis. Only significantly enriched terms are shown, bars depict the fold enrichment over background (human proteome), and the numbers indicate the FDR as determined on https://geneontology.org/. (C) Same as (B) but for factors depleted from HspB2 condensates (red in (A)). Four terms are abbreviated due to space constraints (marked with asterisks). Full terms are: * positive regulation of DNA-templated transcription, elongation; ** regulation of transcription elongation from RNA-Pol II promoter, *** positive regulation of transcription by RNA-Pol II; **** negative regulation of transcription by RNA-Pol II. **(D)** Violin plots depicting the percentage distribution of disordered residues per protein in the nuclear proteome (grey; n = 5376), HspB2 condensate components (blue; n = 49), and proteins depleted from HspB2 condensates (red; n = 49) as predicted by the IUPred algorithm. Solid and dashed lines indicate the median and quartiles, respectively; a Kruskal-Wallis test followed by Dunn's multiple comparisons test was used to determine statistical significance (also for (E)). **(E)** Violin plots showing the isoelectric point (pI) of proteins enriched in and depleted from HspB2 condensates, compared to the human proteome reference dataset (grey). **(F)** Confocal microscopy images of HspB2 condensates in HEK293T cells, co-stained with antibodies against indicated proteins. The rectangular inset indicates the area of the image shown enlarged in (G). The scalebar denotes 10 μm.**(G)** Magnification of the inset shown in (F). The arrow indicates the line and direction along which signal intensity was plotted in (H). **(H)** Histogram depicting signal intensities of GFP-HspB2 (green lines) and indicated proteins (red shading) along the arrows shown in (G).

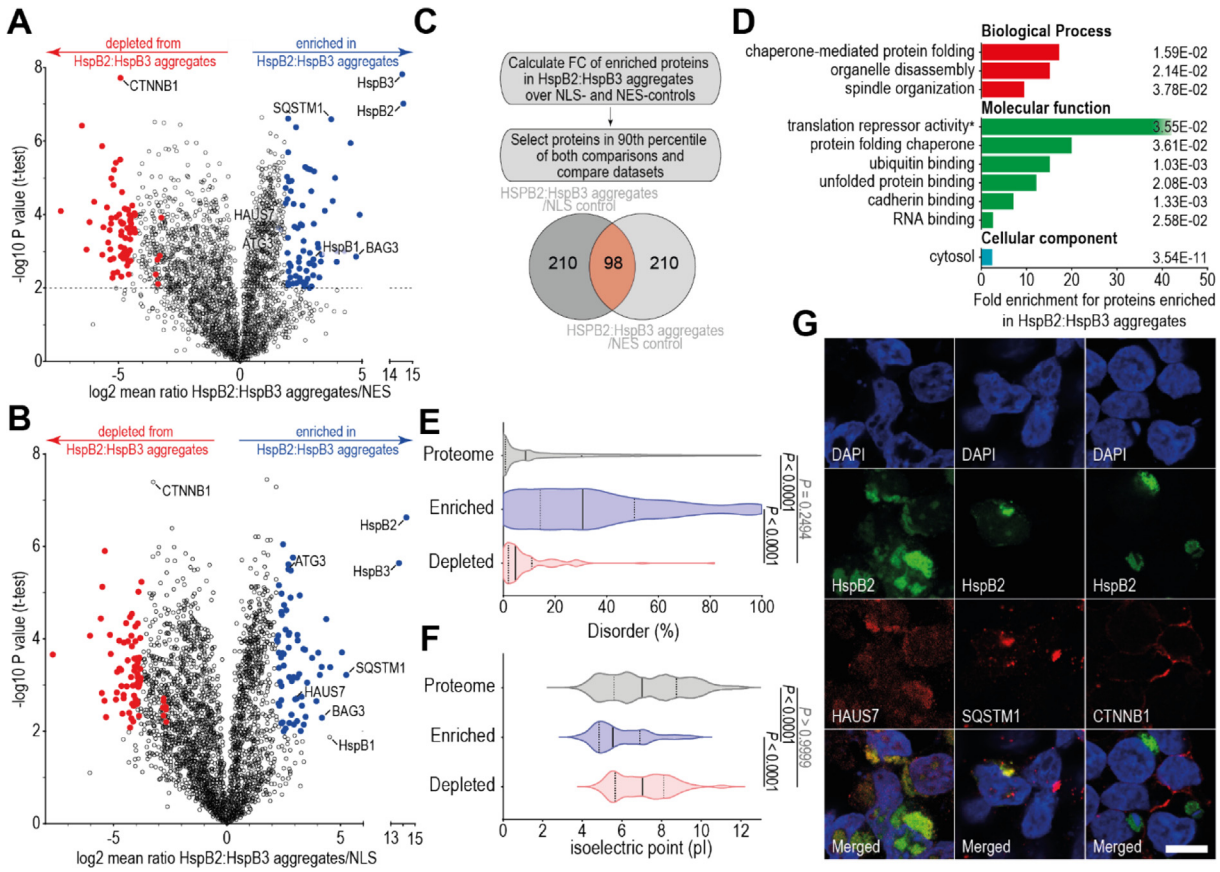

Figure 6. Disordered proteins and autophagy factors are recruited to HspB2:HspB3 aggregates (A-B) Enrichment of biotinylated proteins in HspB2:HspB3 aggregate proximity labelling relative to APEX-NES (A) and APEX-NLS (B) controls. The 5% most enriched and depleted proteins with a *P*-value < 0.01 are shown in blue and red, respectively. **(C)** Overview of the method used to select a high-confidence set of proteins associated with HspB2:HspB3 aggregates by comparing against two different control datasets. **(D)** Gene onthology (GO)-term enrichment analysis of the proteins identified in (C) as determined using the https://geneontology.org/ webtool. Only significant term are shown, numbers indicate the FDR. * GO-term abbreviated, full term: 'translation repressor activity, mRNA regulatory element binding'. **(E)** Violin plots displaying the distribution of protein disorder in the human proteome (grey; n = 61403), proteins enriched (blue; n = 98) and depleted (red; n = 87) in HspB2:HspB3 aggregates as predicted by IUPred. The median and quartiles are indicated by solid and dashed lines, respectively; to test for significance, a Kruskal-Wallis test followed by Dunn's test for multiple comparisons was used (also for (F)). **(F)** Violin plots displaying the distribution of isoelectric points (pI) of proteins enriched in (blue) and depleted from (red) HspB2:HspB3 aggregates, compared to the whole proteome reference dataset (grey). **(G)** Confocal images of HEK293T cells containing (GFP)-HspB2:HspB3 aggregates, co-stained with antibodies targeting indicated interactors.

(8-fold (vs. NES)/43-fold (vs. NLS)) were also enriched in HspB2:HspB3 aggregates. We identified the top 10% enriched proteins relative to both APEX-NES and APEX-NLS controls, and selected those proteins (n = 98) present in both comparisons for GO-term enrichment analysis (Figure 6(C), listed in Table S1C). This analysis revealed an enrichment of factors associated with chaperone-assisted protein folding (Figure 6(D)). In line with this, the amount of disorder in proteins enriched in HspB2:HspB3 aggregates is dramatically higher compared to the proteome reference dataset (median disorder 30.7% vs. 8.6%, respectively; Figure 6(E)), suggesting that many disordered and/or misfolded proteins are associated with these aggregates. We also evaluated the isoelectric points (pI) of selected enriched and depleted proteins, and found that HspB2:HspB3 aggregates are strongly enriched for proteins with a relatively low pI (Figure 6(F)). A lack of correlation between disorder and isoelectric point suggests that both properties contribute independently to a proteins uptake by HspB2 condensates (Figure S7(E)), or HspB2:HspB3 aggregates (Figure S7(F)).

As observed previously for HspB2 condensates, proteins involved in the organization of the mitotic spindle are enriched in HspB2:HspB3 aggregates (Figure 6(D)). Moreover, enrichment of both RNA binding proteins and proteins involved in

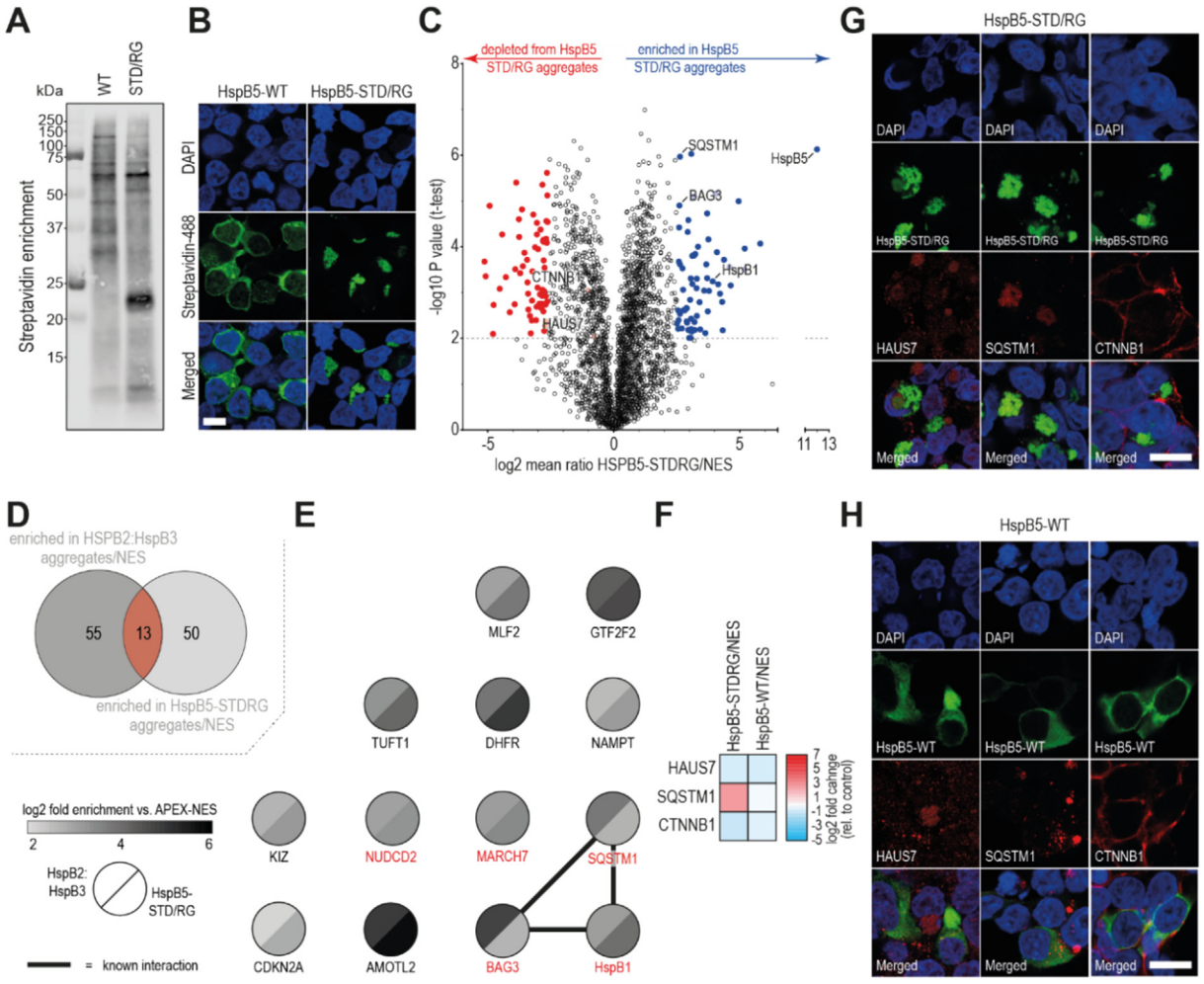

Figure 7. A common set of autophagy factors is recruited to HspB2:HspB3- and HspB5-STD/RG-aggregates
(A) Streptavidin-blotting of enriched biotinylated proteins from HEK293T cells expressing APEX-tagged wildtype (WT) and mutant (STD/RG) HspB5. **(B)** Confocal microscopy images of biotinylation in HEK293T cells expressing APEX-tagged WT and mutant (STD/RG) HspB5. An Alexa488 fluorophore-coupled streptavidin was used to visualize biotinylation. Scale bar is 10 μm. **(C)** Volcano plot showing proteins enriched (blue) and depleted (red) in HspB5-STD/RG aggregate proximity labelling relative to APEX-NES. The top 5% enriched and depleted proteins with a *P*-value < 0.01 are highlighted in blue and red, respectively. **(D)** The overlap between the top 5% enriched factors with a *P*-value < 0.01 in HspB2:HspB3 and HspB5-STD/RG aggregate datasets was determined to uncover common factors enriched in both datasets. **(E)** Schematic overview of the enrichments over APEX-NES of the 13 common factors identified in (D). Grey shading indicates the enrichment in HspB2:HspB3 (top left) and HspB5-STD/RG (bottom right) aggregate datasets. Black lines indicate known physical interactions, and red font indicates proteins linked to GO-terms associated with protein (mis)folding, ubiquitination, ubiquitin binding and/or autophagy. **(F)** Summary of the log2 fold changes of three candidate proteins in HspB5-STD/RG and -WT proximity labelling datasets. **(G-H)** Confocal microscopy images of (GFP-)tagged HspB5-STD/RG (G) and -WT (H) stained with antibodies against indicated proteins. Scalebars indicate 10 μm.

translation repression suggests that HspB2:HspB3 aggregates may influence RNA processes, analogous to stress granules. Lastly, factors involved in organelle disassembly (autophagy) such as SQSTM1 and ATG3 are strongly enriched (see also Figure 6(A-B)), suggesting that the cell is attempting to clear these aggregates.

Interestingly, significantly more proteins were enriched in HspB2:HspB3 aggregates, as compared to HspB2 condensates (1.2% vs. 0.6%, respectively - Figure S7(C)), indicating that a sizeable group of proteins is effectively trapped within HspB2:HspB3 aggregates. Similarly, an even larger subset of proteins is depleted from aggregates as compared to condensates (8.1% vs. 2.0%), indicating HspB2:HspB3 aggregates may constitute a less favorable environment for a larger group of proteins. Immunofluorescence

colocalization imaging confirms the enrichment of HAUS7 and SQSTM1 in HspB2:HspB3 aggregates (Figure 6(G)), which is in line with their enrichment observed in proximity labelling (Figure 6(A-B)). The strong enrichment of disordered proteins in HspB2:HspB3 aggregates combined with the general lack of strongly enriched proteins in HspB2 condensates suggests that HspB2:HspB3 oligomeric complexes bind their substrates more tightly than those consisting only of HspB2. As such, HspB3 may be involved in regulating the sequestrase activity of HspB2.

HspB5-STD/RG and HspB2:HspB3 aggregates sequester a similar autophagy machinery

To enable comparison with another aggregation prone sHSP, we concurrently performed proximity labelling of aggregates formed by a HspB5-mutant (HspB5-STD/RG), which contains both the arginine to glycine substitution at position 120 (R120G) that causes desmin-related cardiomyopathy[45–46] and three serine to aspartic acid phosphomimicking mutations at positions 19, 45 and 59 (S19D, S45D, S59D). Prior work has shown that this mutant accumulates in cytoplasmic aggregates,[47] similar to those seen for HspB2:HspB3. Mapping the composition of two types of sHSP-containing aggregates enables the identification of common factors recruited to such structures.

Proximity labelling in cells transfected with APEX-tagged HspB5-WT and -STD/RG constructs resulted in distinct biotinylation patterns (Figure 7(A)). Biotinylation in HspB5-WT cells localized diffusely in the cytoplasm, while in HspB5-STD/RG cells, amorphous cytoplasmic aggregates were observed (Figure 7(B)). As HspB5-STD/RG is exclusively cytoplasmic, we determined enrichment and depletion of biotinylated proteins relative to the APEX-NES control (Figure 7(C), enriched and depleted proteins are listed in Table S1D-E). HspB5 was enriched strongly (1200-fold), indicating that proximity labelling was successful.

Strikingly, numerous proteins that were found in HspB2:HspB3 aggregates were also enriched in HspB5-STD/RG proximity labelling, including SQSTM1, BAG3, and HspB1 (Figure 7(C)). This prompted us to overlap the sets of enriched proteins in HspB2:HspB3- and HspB5-STD/RG aggregates to identify common factors. We selected the top 5% enriched proteins with a *P*-value < 0.01 from both datasets relative to APEX-NES control and selected common factors (n = 13; Figure 7(D)). Among these common factors were several proteins known to be involved in protein folding, ubiquitination and autophagy (Figure 7(E)). These findings suggest that a common machinery is recruited to aggregates nucleated by different small heat shock proteins. As expected from their enrichment patterns in proximity labelling (Figure 7(F)), SQSTM1 colocalizes with HspB5-STD/RG aggregates (Figure 7(G)), while no specific colocalization is observed with HspB5-WT (Figure 7(H)). Similarly, HAUS7 and CTNNB1 are absent from HspB5-STD/RG aggregates, which is in line with their depletion in proximity labelling.

Discussion

Small heat shock proteins (sHSPs) are the most ubiquitous class of molecular chaperones, and are conserved across all branches of life.[48] A key characteristic of sHSPs is that they assemble into polydisperse, homo- and hetero-oligomeric assemblies of varying conformations and sizes.[14–15] It is widely believed that smaller oligomers are more active as chaperones, while larger oligomers likely function as storage complexes.[49] Interestingly, the chaperone activity of sHSPs can be dynamically regulated by shifting the equilibrium between different sHSPs.[21] To investigate the effects of shifting the balance between components of sHSP hetero-oligomers inside living cells, we focused on HspB2 and HspB3, two chaperones with overlapping tissue expression patterns that have been shown to directly interact[18–20] and co-assemble at a well-defined 3:1 ratio in vitro.[20]

In this study, we explored the effect of changing HspB2:HspB3 expression ratios on the subcellular localization and phase behavior of these proteins inside living cells. To ensure optimal control over relative HspB2 and HspB3 expression levels without the need for suboptimal knockdown or laborious knockout approaches, we used HEK293T cells, as these cells do not express HspB2 and HspB3 endogenously.[50] This experimental set-up therefore provided a clean slate for the study of the effects of stoichiometric shifts in the HspB2:HspB3 balance. We assessed the effects of altering intracellular HspB2:HspB3 ratios by transfecting plasmid DNA encoding these chaperones at various ratios. While the observed protein expression levels roughly matched the ratio of transfected plasmid DNA, this correlation was not linear (Figure S3(A-D)). Upon transfection in HEK293T cells, HspB2 and HspB3 levels are roughly ten times higher than the amount detected in rat hearts,[11] in which these proteins are endogenously expressed, indicating that our HEK293T cell model is likely an overexpression system. While the same amount of total plasmid DNA was transfected in all instances, protein overexpression effects might contribute to the observed phenotypes, as empty vector control plasmids were used as 'filler' DNA. Regardless, we observed highly robust phenotypic differences between cells expressing only HspB2 (HspB2 condensates), and cells co-expressing a moderate (diffuse nuclear HspB2 distribution) or high amount of HspB3 (HspB2:HspB3 aggregates). Our cell model therefore provides an experimentally amenable and tunable system to

trigger condensate and aggregate formation inside living cells. Yet, as interactions with client proteins and other interacting proteins may affect the phase separation behavior of chaperone proteins, the physicochemical properties of HspB2 condensates and HspB2:HspB3 aggregates may differ from those of other protein systems. In addition, as HspB2 is not expressed endogenously in HEK293T cells, mapping its interactome in these cells might yield non-physiological interactions (false positives) or missed interactions of physiological substrates that are not expressed in HEK293T cells (false negatives). Reassuringly, most strong interactors identified in this study (HspB1, BAG3, SQSTM1, and HAUS1, −7, and −8) are highly expressed in muscle tissues.[42] The physiological relevance of these interactions however, should be verified in a system which expresses HspB2 and HspB3 endogenously, such as LHCNM2 or C2C12 cells. Yet, as these cell lines are relatively difficult to culture and transfect, interactome studies in the experimentally amenable HEK293T cell system provide an excellent starting point.

Numerous studies have shown that homo- and hetero-oligomeric sHSP assemblies dramatically differ in their chaperone activity.[21,51–52] For instance, while HspB2 and HspB3 homo-oligomers display moderate chaperone activities,[53–55] HspB2:HspB3 hetero-oligomers have poor chaperone activity.[20] In contrast, hetero-oligomers of HspB4 and HspB5 outperform homo-oligomers consisting of either of the two proteins in chaperone activity assays,[56] and hetero-oligomerization with HspB6 increases chaperone activity of HspB5.[21] While such insights are invaluable, these studies rely on in vitro incubation of purified chaperones with client proteins, thus ignoring the complexity of the cellular environment in which these proteins naturally operate. Our experimental approach of controllable sHSP expression in HEK293T cells can be used to investigate sHSP oligomer assembly inside living cells. HspB2 readily phase separates into nuclear droplets in a concentration-dependent manner in HEK293T cells (this study), as well as in differentiating myoblasts and HeLa cells,[18] suggesting that condensate formation is an intrinsic feature of HspB2. Yet, the latter study also reported the accumulation of overexpressed HspB2 in large amorphous, solid-like intranuclear compartments, which were not observed in our study. Moreover, Lamin A is sequestered inside HspB2 compartments in differentiating myoblasts,[18] but not in HspB2 condensates in HEK293T cells. These findings suggest that HspB2 phase behavior is, in part, cell type specific, which may result from variations in the expression patterns of interacting proteins (such as Lamin A) and other biomolecules, as has been shown previously for other interaction networks.[57–59]

Other sHSPs have been found in condensates or condensate-like structures. For instance, HspB1 and HspB8 locate to stress granules upon proteotoxic stress,[60] and both HspB7 and pseudophosphorylated HspB5 are found in nuclear granules.[36,61] However, condensate formation induced solely by overexpression is a unique feature of HspB2. The reason why HspB2 is able to form condensates on its own remains unclear, but may be related to another unique feature of HspB2, namely its ability to form HspB2/HspB3 tetramers with an anomalous 3:1 ratio. The formation of this unusual tetrameric conformation may require attractive homotypic HspB2-HspB2 interactions that could also underlie condensate formation in the absence of HspB3.

Phase separated condensates are widely believed to sequester and bring together biochemical components within cells.[62–63] It is therefore tempting to speculate that HspB2 condensates may concentrate chaperones and clients to promote chaperone-guided protein refolding. Arguing against this hypothesis, however, is the fact that traditional chaperone clients such as FUS and α-synuclein are not enriched in HspB2 condensates. It is more likely that HspB2 condensates serve as a way to prevent potential toxic effects of excessive HspB2 levels in absence of its partner HspB3. In addition, HspB2 condensates may serve as nuclear chaperone storage pools, from which HspB2 can rapidly be released in times of stress. It is however important to verify this hypothesis in cells that endogenously express HspB2 at physiological levels.

Co-expression of an intermediate amount of HspB3 prevented HspB2 phase separation, while addition of a larger amount triggered the formation of large cytoplasmic and nuclear aggregates. These findings illustrate the dramatic effects of stoichiometric shifts in hetero-oligomer composition, and underscore the importance of maintaining the correct expression balance for sHSP physiological functioning. Remarkably, we observed no obvious detrimental effects on cell survival and proliferation, suggesting that both structures are tolerated by the cells. HspB2 condensates can be dissolved in situ by expression of HspB3 at a later stage, showing that HspB2 condensates are reversible and exchange biomolecules with their surroundings. To our surprise, we found that HspB2:HspB3 aggregates can also be dissolved by shifting the stoichiometry towards HspB2, indicating that formation of these solid-like structures is also reversible, at least in the timeframe we monitored. These results show that both condensates and aggregates are likely formed by transient, weak interactions with other cellular proteins. Whether the observed structures may have longer-term toxic effects remains to be seen.

APEX-mediated proximity labelling of HspB2 condensates revealed that only few of the detected proteins are strongly enriched in, or depleted from HspB2 condensates, suggesting that most proteins are able to freely diffuse in and out of these droplets, without getting trapped. In comparison, substantially more proteins are enriched in, and depleted from solid-like HspB2:HspB3 and HspB5-STD/RG aggregates, indicating subsets of proteins are specifically trapped inside these structures. Interestingly, a specific group of proteins is enriched in both HspB2:HspB3 and HspB5-STD/RG aggregates. This group includes proteins involved in ubiquitination and autophagy including SQSTM1, and may therefore represent a common molecular machinery aimed at clearing sHSP aggregates. SQSTM1 accumulation has previously been observed in HspB5-STD/RG aggregates,[64] and is often interpreted as a marker for defects in autophagic degradation.[65–66] Whether autophagy of the sHSP aggregates observed here is effective, or inhibited because of entrapment of these factors within aggregates remains to be explored.

In differentiating myoblasts, HspB2 subcellular localization is highly heterogeneous, ranging from nuclear condensates and diffuse distribution, to amorphous compartments.[18] This dramatic phenotypical variation likely stems from cell-to-cell variation in the differentiation stage and related HspB2:HspB3 expression levels. The HEK293T cell platform we developed here allows more control over relative sHSP expression levels, enabling the study of sHSP structures with uniform biophysical properties and subcellular localization phenotypes. As such, this approach allowed us to map the composition of HspB2 condensates and HspB2:HspB3 aggregates, as well as HspB5-STD/RG aggregates. We anticipate that our approach can be used for the study of biophysical properties and composition of other sHSP structures, as well as the investigation of the effects of disease-related sHSP mutants.[67] Our findings may help shed light on the origins of phenotypes associated with mutations in sHSPs that cause inclusion bodies, and improve our understanding of the functions and mechanisms of sHSPs.

Materials and methods

Analysis of sHSP expression

For the generation of the sHSP expression heatmaps depicted in Figure S1, RNA and protein expression data was extracted from the Human Protein Atlas (www.proteinatlas.org).[42] The extracted RNA-expression data is a consensus dataset derived from the RNA-seq dataset generated internally by the Human Protein Atlas (HPA), RNA-seq data from the Genotype-Tissue Expression (GTEx) project, and CAGE data from the FANTOM5 project. Expression values from the three datasets were normalized to generate the Normalized eXpression (NX) values depicted in Figure S1(-A-B). For the tissue enrichment analysis, a pseudocount of 0.1 was added to all NX-values. This tissue-specific expression values were subsequently divided by the average sHSP expression value across all tissues as a measure of tissue-specific enrichment. The data was then log2 transformed to produce the heatmap depicted in Figure S1(C). Protein expression data is derived from immunohistochemically stained tissues, using four levels of expression (high, medium, low, and not detected).

Protein disorder and isoelectric point prediction

To predict intrinsically disordered regions within HspB2 and candidate proteins, we used IUPred 3 (https://iupred3.elte.hu/),[68] using default settings. The percentage of disorder for groups of proteins identified by mass spectrometry, as well as for the entire human proteome was extracted from the Disorder Atlas (https://disorderatlas.med.umich.edu/index)[69–70], which makes use of the IUPred prediction algorithm.[71–72]

To determine the isoelectric points (pI) of candidate proteins, we extracted the average pI as determined by 17 different methods.[73] In cases where multiple isoforms of the same protein were detected by mass spectrometry, only those that had at least half of the peptides relative to the leading protein were retained for determination of the pI.

Culturing and transfecting HEK293T cells

HEK293T cells were maintained in DMEM supplemented with 10% fetal bovine serum (Sigma, #F0804) and 1% Penicillin/Streptoymycin (HyClone, SV30010) at 37 °C and 5% CO_2. Cells were detached using Trypsin/EDTA (0.25%/0.02%) and passaged two times per week at a 1:10 to 1:20 ratio, depending on confluency.

For transfection of HEK293T cells seeded into a single well of a 24-wells plate (culture volume 500 μL), 500 ng plasmid DNA was combined with 1.5 μL polyethyleneimine (PEI, 1 mg/mL, Sigma, #p3143) in 50 μL Optimem (Gibco, #31985070). The transfection mixture was incubated at room temperature for 30 minutes before being added dropwise to the cells. For larger culture volumes, the amount of plasmid DNA, PEI, and Optimem was increased proportionally. HspB2- and HspB3-encoding plasmids were transfected at 9:0 and 9:1 ratios to trigger the formation of HspB2 condensates and diffuse nuclear HspB2 distribution, respectively. To trigger formation of HspB2:HspB3 aggregates, plasmids were transfected at an equimolar 9:9 ratio, apart from the experiments in Figures 2(G-I) and S3(F), where a 9:3 ratio was used to trigger aggregate formation.

Live cell imaging

All live cell imaging was performed at 37 °C on the Leica DMi8 widefield microscope in Cellvis glass bottom dishes (cat# D60-30-1.5-N). During live imaging experiments, HEPES was added to the culture medium to an end concentration of 25 mM to control fluctuations in pH in the absence of CO_2. Thunder computational clearing and widefield deconvolution was applied to live imaging data for background subtraction. For Videos S1-4, bleach correction was performed in Fiji (Image > Adjust > Bleach Correction > Histogram Matching) to correct for signal decay due to high scanning frequency.

Quantification of sHSP protein production after transfection

Purified recombinant HspB2 protein and HspB2:HspB3 3:1 protein complexes were analyzed for purity with Coomassie staining.[20] These purified proteins were used to make standard curves against which HspB2 and HspB3 protein levels in transfected HEK293T cell lysates were quantified. In parallel, transfection efficiency was determined by transfected the biotin ligase ultraID[74] fused to a nuclear localization signal. After ultraID mediated biotinylation, transfected cells could be readily detected using an Alexa488 fluorophore coupled streptavidin. Subsequently, relative and absolute protein content was determined by combining the outcomes of the abovementioned methods to determine protein levels and transfection efficiency with the number of cells underlying these lysates (as quantified using the Luna classic cell counter prior to lysis) and the total protein content of the lysate (as determined by BCA assay).

Fluorescence recovery after photobleaching (FRAP)

HEK293T cells containing HspB2 condensates and HspB2:HspB3 aggregates were imaged under an Olympus IX81 spinning disk confocal microscope, equipped with an Andor FRAPPA photobleach module and Yokogawa CSU-X1 spinning disk. The Andor 400 series solid-state lasers were used to bleach and image the samples. All images were recorded using a 100 × oil immersion objective (numerical aperture 1.5) and an Andor iXon3 EM CCD camera. After taking an initial pre-bleach image, identified condensates and aggregates were partially bleached using a single iteration of 100% laser power, after which post-bleach images were acquired every 250 ms and 1000 ms for condensates and aggregates, respectively.

Immunofluorescence analysis

Coverslips were sterilized with 100% ethanol prior to coating with poly-L-lysine (0.1 mg/mL) for 5 minutes at room temperature. After thorough rinsing with milli-Q, coverslips were allowed to dry for at least two hours before seeding HEK293T cells as described above. Approximately 16 hours after seeding, cells were transfected as described above. 24 hours after transfection, cells were fixed in 4% paraformaldehyde (PFA; Fluka-#47629), supplemented with 0.1% SDS, 0.5% sodium deoxycholate and 1% Triton. After fixation, cells were washed three times with PBS before incubating with 200 μL ice-cold acetone for 5 minutes. After two washes with PBS, cells were either stored under PBS-Glycine (10 mM) at 4 °C or directly stained as below.

Subsequently, cells were treated with 0.25% Triton in PBS for 20 minutes. Cells were subsequently washed with PBS and incubated in blocking buffer (3% BSA, 0.1% Triton, 10% normal goat serum in PBS) supplemented with 100 mM glycine for 30 minutes. After blocking, cells were incubated with primary antibodies (all at 1:100 dilution unless noted otherwise) in blocking buffer for 1 hour at room temperature. Primary antibodies used in immunofluorescence experiments were rabbit-anti-HspB2 (generated in our laboratory,[75,76] mouse-anti-myc (Thermo Fisher Scientific Cat# MA1-980, RRID:AB_558470), mouse-anti-Lamin A (Nordic-MUbio, cat# 1101P), rabbit-anti-Lamin B1 (Proteintech, cat# 12987-1-AP, RRID:AB_2136290), mouse-anti-SQSTM1 (Santa Cruz Biotechnology, cat# sc-28359, RRID:AB_628279), mouse-anti-HAUS7 (Santa Cruz Biotechnology, cat# sc-393259), mouse-anti-CTNNB1 (Santa Cruz Biotechnology, cat# sc-7963, RRID:AB_626807), mouse-anti-SC-35 (Sigma-Aldrich Cat# S4045, RRID:AB_477511), mouse-anti-PML (1:5;[77]). After incubation with primary antibodies, coverslips were washed three times using 0.05% Tween in PBS for 5 minutes before incubation with secondary antibodies (all at 1:100 dilution) in blocking buffer for 1 hour at room temperature. Secondary antibodies used in immunofluorescence experiments were goat-anti-mouse Alexa 568 (Thermo Fisher Scientific Cat# A-11004, RRID:AB_2534072) and goat-anti-rabbit Alexa647 (Thermo Fisher Scientific Cat# A27040, RRID:AB_2536101). Where indicated, biotinylated proteins were visualized using a streptavidin-alexa488 conjugate (Invitrogen, #S32354). Subsequently, cells were washed twice with 0.05% Tween in PBS and twice with PBS before nuclei were counterstained with 1 μg/mL DAPI in PBS for 5 minutes at room temperature. Afterwards, cells were rinsed twice with PBS, once with PBS-milliQ 1:1, and three times with milliQ before mounting in Mowiol (Sigma, #81381). After overnight hardening of the mounting medium at room temperature, microscopy samples were stored at 4 °C.

Imaging of fixed cells

All images of fixed material were generated using the Leica SP8 confocal microscope, except for those shown in Figure S3(F), which were made using the Zeiss Axio Imager fluorescence microscope. The histograms depicting signal intensity in Figures 2(B), 7(C), S3(F), S4(B), and S4(D) were generated using Fiji.[78] Intensity values were optimized using the minimal and maximal intensity values as borders for each channel separately, after which smoothing was applied using a 5-pixel sliding window approach. The myc-HspB3 signal in Figure 3(F) was enhanced in Fiji (Process > Math > Set Gamma to 0.5).

Determination of minimal concentration threshold for condensate formation

To determine the average GFP-HspB2 signal intensity in cells that either did or did not contain condensates, mid- Z-stack optical sections were selected and duplicated in Fiji (Image > Duplicate). This duplicate was converted to 8-bit before a threshold was applied (Image > Adjust > Auto Threshold > Select 'Moments' with default setting). The thresholded, binary duplicate was normalized to 65535 (16bit) and subtracted from the original image using Process > Image Calculator, and the mean intensity value for the GFP-HspB2 signal was determined for individual cells, correcting for the area of the cell that was removed in the previous step. Throughout sample processing, imaging, and image manipulations, the same settings were used for all samples, thus enabling direct comparison between cells.

Determination of circularity of condensates and aggregates

To assess circularity of HspB2 condensates and aggregates, mid Z-stack optical sections were selected and converted to 8-bit. Bernsen local thresholding was performed using Fiji (Image > Adjust > Auto Local Threshold > Bernsen [radius = 100; parameter 1 = 100; parameter 2 = default]). Subsequently, area and circularity of thresholded structures was determined in Fiji (Analyze > Analyze particles [default settings, except size (μm^2) set to 0.08 – infinity).

Automated analysis of HspB2 condensate and aggregate size and localization

For the computational image analysis, python (>3.7, Delaware USA) was used. For the detection of the cells as well as the aggregates and condensates, images were thresholded with a global Otsu filter,[79] after which a cut-off parameter was introduced. The obtained threshold was modified by multiplying its value with the cut-off value to remove weaker signals around the periphery of the aggregates and condensates. Finally, the remaining spurious noise in the image was removed (isolated pixel islands, the filter removes pixels when five neighbouring pixels are zero, the pixel of interest is set to zero as well). These steps generated two parameters (a cut-off and noise removal), which determined the size and shape of the detected aggregates and cells. To estimate the size of the aggregates defined in number of pixels, and to label individual aggregates, all possible graphs of distance for the nodes (all nonzero pixels) in the image matrix were created.[80] Subsequently overlap with the DAPI signal was determined to assess whether the aggregates are located within the nucleus. To justify the final choice for the image analysis parameters (cut-off = 2.25 and noise filter = 5) the filtered images and data analysis for a range of relevant parameter values are shown in Figure S5. The code can be found on the https://github.com/huckgroup.

Flow cytometry proliferation assay

For each condition, 1×10^5 HEK293T cells were seeded in a single well of a 12-wells plate. After overnight incubation, cells were incubated in 100 nM CellTrace violet (Invitrogen, C34557) in PBS for 20 minutes at 37 °C. Subsequently, cells were washed twice with culture medium and fresh culture medium was added. Where specified, cells were transfected with indicated transfection mixes directly after incubation with the CellTrace violet solution. As a control, an empty pIRES vector not encoding HspB2 or HspB3 was used. At indicated time points, cells were washed with PBS and fixed in 4% PFA for 20 minutes. Afterwards, cells were washed once with PBS, resuspended in 200 μL FACS buffer (0.1% BSA, 0.05% NaN_3, 0.5 mM EDTA in PBS), and stored at 4 °C awaiting FACS analysis. Flow cytometry was performed on a FACSVerse (BD Biosciences) flow cytometer. CellTrace violet was detected using the 405 nm laser line and the 448/45 filter, GFP-HspB2 was detected using the 488 nm laser line and the 510/20 filter. For the plots of HspB2-transfected cells shown in Figure S3(E), only GFP-positive cells were analyzed to correct for variations in transfection efficiency.

Fractionation of soluble and insoluble fractions

Cells grown in 12 wells plates were harvested using trypsin and pelleted by centrifuging at 1500 × *g* for 5 minutes at room temperature. Subsequently, cells were washed once with PBS, split into two replicate samples, and pelleted as before. The cell pellet of one replicate was lysed directly in 9 μL 4x SDS sample buffer (62.5 mM Tris-HCl [pH 6.8], 2% SDS, 5% β-mercaptoethanol, 10% glycerol, 0.005%

bromophenol blue) to serve as total fraction. The other replicate was lysed in 25 μL RIPA lysis buffer (50 mM Tris-HCl [pH 7.5], 150 mM NaCl, 0.1% SDS, 0.5% sodium deoxycholate, 1% Triton X-100, 1x cOmplete protease inhibitor cocktail [Roche-11697498001], 1 mM PMSF), incubated on ice for 10 minutes and centrifuged for 10 minutes at 21100 × *g* at 4 °C. Subsequently, the supernatant was combined with 9 μL 4x SDS sample buffer to constitute the soluble fraction, while the insoluble pellet was washed once in RIPA buffer before adding 25 μL milliQ and 9 μL 4x SDS sample buffer. All samples were subsequently heated for 10 minutes at 95 °C.

Western blotting

Samples were size separated on 12.5% polyacrylamide gels, transferred into nitrocellulose membranes and blocked with 5% w/v nonfat dry milk in PBS for 30 minutes at room temperature. In cases where membranes were stained for biotin, 3% BSA in TBST was used for blocking and as diluent for subsequent antibody incubations. After blocking, membranes were incubated for 1 hour at room temperature with indicated primary antibodies (rabbit-anti-HspB2 [generated in our laboratory; 1:1000], rabbit-anti-HspB3 [generated in our laboratory; 1:1000],[75] mouse-anti-tubulin-β (DSHB cat# E7, RRID: AB_528499; 1:1000]) diluted in 2.5% w/v nonfat dry milk in PBST. After extensive washing using PBST, membranes were incubated for 1 hour with secondary antibodies (goat-anti-rabbit-IRDye680 [Li-Cor Biosciences cat# 926-68071, RRID: AB_10956166], goat-anti-mouse-IRDye800 [Li-Cor Biosciences cat# 926-32210, RRID: AB_621842]) both at 1:10000 in 2.5% w/v nonfat dry milk in PBST. Afterwards, membranes were washed extensively in PBST again and imaged using the Li-Cor Odyssey CLx.

For quantification of western blot signals in Figure 2(H), intensity values were normalized using the tubulin-β signals of total samples to account for minor variations during cell culture, lysis and gel loading. Subsequently, the amount of HspB2 in the insoluble pellet fraction was calculated and expressed as a percentage relative to the HspB2 signal in the total sample.

APEX proximity labelling

Proximity labelling was performed as described in.[22] In brief, the APEX2-tag was amplified from the APEX2-NLS plasmid gifted by Alice Ting (Addgene plasmid # 124617) and introduced into pcDNA5 expression vectors, containing genes encoding HspB2, HspB5-WT, -STD/RG, and nuclear export/nuclear localization signals as indicated. Subsequently, these plasmids were transfected into HEK293T cells using PEI as described previously. 24 hours after transfection, cells were incubated in 500 μM biotin-phenol (BP) in full DMEM for 45 minutes at 37 °C. Next, a fresh 100x stock of 100 mM H_2O_2 in PBS was prepared, and H_2O_2 was directly added to the BP-solution to a final concentration of 1 mM. Cells were incubated for 1 minute, after which the labelling solution was removed. Cells were washed three times in quencher solution (10 mM sodium ascorbate, 5 mM trolox and 10 mM sodium azide in PBS) before fixation or cell lysis.

Preparation of lysates for mass spectrometry

Plasmids encoding indicated APEX-tagged transgenes and untagged genes were transfected into HEK293T cells. For each lysate, 70 μg total plasmid DNA was used to transfect two T175 flasks seeded with HEK293T cells at approximately 70% confluency (See Figure S6(A) for exact composition of transfection mixes). 24 hours after transfection, APEX-proximity labelling was performed as above. After labelling, medium was removed and cells were washed twice with quencher solution, and twice with PBS, followed by a final wash with quencher solution. Each wash was performed for 1 minute, using 25 mL of wash solution. After the final wash, cells were harvested in quencher solution (10 mL per T175) using a cell scraper, transferred to 50 mL Falcon tubes and placed on ice. After all samples were harvested, cells were centrifuged at 3000 × *g* for 20 minutes at 4 °C. Cell pellets were resuspended in 1 mL PBS, transferred to Eppendorf tubes, and centrifuged for 2 minutes at 1500 × *g*. Cell pellets were resuspended in 120 μL lysis buffer 1 (1% SDS, 1 mM DTT, 1x complete protease inhibitors, 1 mM PMSF, 10 mM sodium ascorbate, 5 mM trolox, 10 mM sodium azide) and heated at 90 °C to promote solubilization of aggregated proteins. Subsequently, lysates were sonicated three times using a 30 sec on/30 sec off protocol. Next, lysates were diluted by adding 1080 μL lysis buffer 2 (56 mM Tris-HCl [pH 7.5], 167 mM NaCl, 0.55% NP-40, 0.55% sodium deoxycholate, 1x complete protease inhibitors, 1 mM PMSF, 10 mM sodium ascorbate, 5 mM trolox, 10 mM sodium azide) and sonicated as before. Lysates were cleared by centrifugation at 21100 × *g*, 4 °C for 10 minutes. Supernatants were taken and dialyzed using Slide-A-Lyzer (Thermo, #66332) cassettes to remove free biotin-phenol. Briefly, the membranes were hydrated, after which the samples were loaded and dialyzed in 3 L dialysis buffer (50 mM Tris-HCl [pH 7.5], 150 mM NaCl, 1 mM DTT) for 2 hours at 4 °C. After 2 hours, dialysis buffer was refreshed and samples were dialyzed for an additional 2 hours. Subsequently, dialysis buffer was refreshed once more, and samples were incubated overnight. The following day, lysates were recovered, transferred to Eppendorf tubes and glycerol was added to a final concentration of 10%. After setting aside small fractions of each

sample for Bradford assay and a small scale streptavidin enrichment test, lysates were snap-frozen in liquid nitrogen and stored at −80 °C. Protein concentration was determined using Bradford assay.

Streptavidin enrichment and on-bead digestion

Throughout streptavidin enrichment and washing procedures, samples were kept on ice as much as possible. Streptavidin Sepharose High Performance beads (Cytiva, #17-5113-01) were equilibrated in IP-buffer (50 mM Tris-HCl [pH 7.5], 150 mM NaCl, 0.5% NP-40, 0.5% sodium deoxycholate, 0.1% SDS, 0.5 mM DTT, 1 × cOmplete protease inhibitor cocktail, 1 mM PMSF, 10 mM sodium ascorbate, 5 mM trolox, 10 mM sodium azide) three times, with centrifugation at room temperature for 2 minutes at 2000 × *g* in between. For each streptavidin enrichment, 15 μL bead slurry was used. Purification was performed in triplicate by combining 400 μg protein lysate in IP-buffer and equilibrated bead suspension in a total volume of 500 μL per replicate. In addition, 20μg ethidium bromide was added to prevent indirect, DNA-mediated interactions. Samples were incubated for 90 minutes at 4 °C with end-over-end rotation. Subsequently, beads were washed twice with wash buffer (25 mM Tris-HCl [pH 7.5], 150 mM NaCl, 1% NP-40, 1% sodium deoxycholate, 0.1% SDS, 0.5 mM DTT, 1 × cOmplete protease inhibitor cocktail, 1 mM PMSF), twice with 1% NP-40 in PBS (MS-grade) and twice with PBS (MS-grade). From this point onwards, all incubations and centrifugation steps were performed at room temperature. The final wash was removed completely using an insulin syringe (BD cat# 324825, gauge 30), beads resuspended in 50 μL freshly prepared elution buffer 1 (2 M urea, 100 mM Tris-HCl [pH 8.0], 10 mM DTT) and incubated for 20 minutes in a thermoshaker set to 1250 rpm. Iodoacetamide was added to a final concentration of 50 mM and samples were incubated for an additional 10 minutes on the thermoshaker. After addition of iodoacetamide, samples were kept in the dark as much as possible. Subsequently, 0.25 μg trypsin (Promega, V5111C) was added and bead suspensions were incubated for approximately 150 minutes on the thermoshaker at 1250 rpm. After centrifugation for 2 minutes at 2000 × *g*, the supernatant containing tryptic peptides was taken and transferred to a new Eppendorf tube. Next, 50 μL freshly prepared elution buffer 2 (2 M urea, 100 mM Tris-HCl [pH 8.0]) was added to the beads, which were subsequently incubated for 5 minutes at 1250 rpm on the thermoshaker. Again, beads were pelleted by centrifugation (2minutes,2000xg), supernatant was collected and combined with the supernatant taken previously. Combined supernatants were incubated overnight at room temperature after addition of 0.1 μg trypsin. Samples were acidified by adding 10 μL trifluoroacetic acid (10%), purified and desalted on C18 StageTips[81] and stored at 4 °C until measurement on the mass spectrometer.

Mass spectrometry

Peptides were separated through reverse phase nano-HPLC on an Easy-nLC 1000 (Thermo Fisher) coupled on-line to a Thermo Fisher Orbitrap Exploris 480 mass spectrometer. A 60 minute gradient of buffer B (80% acetonitrile, 0.1% formic acid) was applied and the mass spectrometer was run in Top20 mode. After fragmentation, peptides were added to a dynamic exclusion list for 45 seconds.

Mass Spectrometry data analyses

The RAW data have been analyzed using MaxQuant version 1.6.6.0[82] LFQ and iBAQ settings enabled, and deamidation (NQ) added as variable modification. The database was downloaded from UniProtKB in June 2017 and APEX protein sequences were added. The raw mass spectrometry data and Maxquant output have been deposited to the ProteomeXchange Consortium via the PRIDE[83] partner repository with the dataset identifier PXD035040. Raw MS dataset identifiers of individual triplicates are indicated in Figure S6(A).

Mapped mass spectrometry data was processed using Perseus 1.5.0.15.[84] In brief, identified proteins were filtered for contaminants and reverse hits, after which LFQ-values were log2-transformed. Samples were grouped into triplicates and filtered to contain three valid values in at least one group of replicates. Missing values were subsequently imputed assuming normal distribution to allow statistical analyses. Volcano plots were generated in Perseus and replotted in GraphPad Prism 8. GO-term analysis of proteins enriched in HspB2 condensates and HspB5-STD/RG aggregates was performed on proteins in the 95th percentile with $P < 0.01$ in the appropriate comparison. Similarly, for the analysis of proteins depleted in HspB2 condensates, the 5% most depleted proteins with a *P*-value < 0.01 were selected. To investigate GO-term enrichment of factors enriched in HspB2:HspB3 aggregates, proteins in the 90th percentile relative to both APEX-NES and -NLS controls were selected. These datasets were then overlapped and only those proteins present in both comparisons were selected for GO-term enrichment analysis. GO-term enrichment analysis[85–87] was performed by testing lists of selected proteins against the human proteome reference list on http://geneontology.org/. Only enriched terms with an FDR $P < 0.05$ are shown.

CRediT authorship contribution statement

Joep Joosten: Conceptualization, Methodology, Validation, Formal analysis, Investigation, Writing – original draft, Writing – review & editing, Visualization, Supervision. **Bob van Sluijs:** Software. **Wilma Vree Egberts:** Validation, Investigation. **Martin Emmaneel:** Investigation. **Pascal W.T.C. Jansen:** Formal analysis. **Michiel Vermeulen:** Resources, Supervision. **Wilbert Boelens:** Conceptualization, Resources, Writing – review & editing, Supervision, Funding acquisition. **Kimberly M. Bonger:** Conceptualization, Resources, Supervision, Funding acquisition. **Evan Spruijt:** Conceptualization, Resources, Writing – original draft, Writing – review & editing, Supervision, Funding acquisition.

DATA AVAILABILITY

Data will be made available on request.

DECLARATION OF COMPETING INTEREST

The authors declare that they have no known competing financial interests or personal relationships that could have appeared to influence the work reported in this paper.

Acknowledgements

We thank colleagues from the departments of Biomolecular Chemistry and Physical Organic Chemistry for fruitful discussions. We thank dr. Wolf of the department of Cell Biology, RadboudUMC Nijmegen for kindly providing the Lamin A and Lamin B1 antibodies. We acknowledge dr. Jelle Postma, for his assistance in microscopic imaging. This work was financially supported by the Institute for Molecules and Materials (Radboud University). E.S. acknowledges the Netherlands Organization for Scientific Research (NWO – grant number: 193.089) for funding.

Appendix A. Supplementary Data

Supplementary data to this article can be found online at https://doi.org/10.1016/j.jmb.2023.168139.

Received 22 November 2022;
Accepted 27 April 2023;
Available online 3 May 2023

Keywords:
HspB2;
HspB3;
molecular chaperone;
proximity labeling;
liquid-liquid phase separation

† Equal contribution.

References

1. Hilton, G.R., Lioe, H., Stengel, F., Baldwin, A.J., Benesch, J.L., (2013). Small heat-shock proteins: paramedics of the cell. *Top. Curr. Chem.* **328**, 69–98.
2. Mogk, A., Bukau, B., Kampinga, H.H., (2018). Cellular Handling of Protein Aggregates by Disaggregation Machines. *Mol. Cell* **69**, 214–226.
3. Garrido, C., Paul, C., Seigneuric, R., Kampinga, H.H., (2012). The small heat shock proteins family: the long forgotten chaperones. *Int. J. Biochem. Cell Biol.* **44**, 1588–1592.
4. Parcellier, A., Brunet, M., Schmitt, E., Col, E., Didelot, C., Hammann, A., Nakayama, K., Nakayama, K.I., et al., (2006). HSP27 favors ubiquitination and proteasomal degradation of p27Kip1 and helps S-phase re-entry in stressed cells. *FASEB J.* **20**, 1179–1181.
5. Carra, S., Seguin, S.J., Lambert, H., Landry, J., (2008). HspB8 chaperone activity toward poly(Q)-containing proteins depends on its association with Bag3, a stimulator of macroautophagy. *J. Biol. Chem.* **283**, 1437–1444.
6. Zhang, H., Rajasekaran, N.S., Orosz, A., Xiao, X., Rechsteiner, M., Benjamin, I.J., (2010). Selective degradation of aggregate-prone CryAB mutants by HSPB1 is mediated by ubiquitin-proteasome pathways. *J. Mol. Cell. Cardiol.* **49**, 918–930.
7. Goncalves, C.C., Sharon, I., Schmeing, T.M., Ramos, C.H. I., Young, J.C., (2021). The chaperone HSPB1 prepares protein aggregates for resolubilization by HSP70. *Sci. Rep.* **11**, 17139.
8. Sweeney, P., Park, H., Baumann, M., Dunlop, J., Frydman, J., Kopito, R., McCampbell, A., Leblanc, G., et al., (2017). Protein misfolding in neurodegenerative diseases: implications and strategies. *Transl Neurodegener* **6**, 6.
9. Tedesco, B., Cristofani, R., Ferrari, V., Cozzi, M., Rusmini, P., Casarotto, E., Chierichetti, M., Mina, F., et al., (2022). Insights on Human Small Heat Shock Proteins and Their Alterations in Diseases. *Front. Mol. Biosci.* **9**, 842149.
10. Janowska, M.K., Baughman, H.E.R., Woods, C.N., Klevit, R.E., (2019). Mechanisms of Small Heat Shock Proteins. *Cold Spring Harb Perspect. Biol.* **11**
11. Sugiyama, Y., Suzuki, A., Kishikawa, M., Akutsu, R., Hirose, T., Waye, M.M., Tsui, S.K., Yoshida, S., et al., (2000). Muscle develops a specific form of small heat shock protein complex composed of MKBP/HSPB2 and HSPB3 during myogenic differentiation. *J. Biol. Chem.* **275**, 1095–1104.
12. Iwaki, A., Nagano, T., Nakagawa, M., Iwaki, T., Fukumaki, Y., (1997). Identification and characterization of the gene encoding a new member of the alpha-crystallin/small hsp family, closely linked to the alphaB-crystallin gene in a head-to-head manner. *Genomics* **45**, 386–394.
13. Suzuki, A., Sugiyama, Y., Hayashi, Y., Nyu-i, N., Yoshida, M., Nonaka, I., Ishiura, S., Arahata, K., et al., (1998). MKBP, a novel member of the small heat shock protein

family, binds and activates the myotonic dystrophy protein kinase. *J. Cell Biol.* **140**, 1113–1124.
14. Van Montfort, R., Slingsby, C., Vierling, E., (2001). Structure and function of the small heat shock protein/alpha-crystallin family of molecular chaperones. *Adv. Protein Chem.* **59**, 105–156.
15. Boelens, W.C., (2020). Structural aspects of the human small heat shock proteins related to their functional activities. *Cell Stress Chaperones* **25**, 581–591.
16. Sudnitsyna, M.V., Mymrikov, E.V., Seit-Nebi, A.S., Gusev, N.B., (2012). The role of intrinsically disordered regions in the structure and functioning of small heat shock proteins. *Curr. Protein Pept. Sci.* **13**, 76–85.
17. Martin, E.W., Holehouse, A.S., (2020). Intrinsically disordered protein regions and phase separation: sequence determinants of assembly or lack thereof. *Emerg Top Life Sci* **4**, 307–329.
18. Morelli, F.F., Verbeek, D.S., Bertacchini, J., Vinet, J., Mediani, L., Marmiroli, S., Cenacchi, G., Nasi, M., et al., (2017). Aberrant Compartment Formation by HSPB2 Mislocalizes Lamin A and Compromises Nuclear Integrity and Function. *Cell Rep.* **20**, 2100–2115.
19. Clark, A.R., Vree Egberts, W., Kondrat, F.D.L., Hilton, G. R., Ray, N.J., Cole, A.R., Carver, J.A., Benesch, J.L.P., et al., (2018). Terminal Regions Confer Plasticity to the Tetrameric Assembly of Human HspB2 and HspB3. *J. Mol. Biol.* **430**, 3297–3310.
20. den Engelsman, J., Boros, S., Dankers, P.Y., Kamps, B., Vree Egberts, W.T., Bode, C.S., Lane, L.A., Aquilina, J.A., et al., (2009). The small heat-shock proteins HSPB2 and HSPB3 form well-defined heterooligomers in a unique 3 to 1 subunit ratio. *J. Mol. Biol.* **393**, 1022–1032.
21. Mymrikov, E.V., Riedl, M., Peters, C., Weinkauf, S., Haslbeck, M., Buchner, J., (2020). Regulation of small heat-shock proteins by hetero-oligomer formation. *J. Biol. Chem.* **295**, 158–169.
22. Hung, V., Udeshi, N.D., Lam, S.S., Loh, K.H., Cox, K.J., Pedram, K., Carr, S.A., Ting, A.Y., (2016). Spatially resolved proteomic mapping in living cells with the engineered peroxidase APEX2. *Nat. Protoc.* **11**, 456–475.
23. Dyson, H.J., Wright, P.E., (2005). Intrinsically unstructured proteins and their functions. *Nat. Rev. Mol. Cell Biol.* **6**, 197–208.
24. Wright, P.E., Dyson, H.J., (2015). Intrinsically disordered proteins in cellular signalling and regulation. *Nat. Rev. Mol. Cell Biol.* **16**, 18–29.
25. Banani, S.F., Lee, H.O., Hyman, A.A., Rosen, M.K., (2017). Biomolecular condensates: organizers of cellular biochemistry. *Nat. Rev. Mol. Cell Biol.* **18**, 285–298.
26. Alberti, S., Hyman, A.A., (2021). Biomolecular condensates at the nexus of cellular stress, protein aggregation disease and ageing. *Nat Rev Mol Cell Bio* **22**, 196–213.
27. Dechat, T., Adam, S.A., Taimen, P., Shimi, T., Goldman, R. D., (2010). Nuclear lamins. *Cold Spring Harb. Perspect. Biol.* **2**, a000547.
28. Tiago, T., Hummel, B., Morelli, F.F., Basile, V., Vinet, J., Galli, V., Mediani, L., Antoniani, F., et al., (2021). Small heat-shock protein HSPB3 promotes myogenesis by regulating the lamin B receptor. *Cell Death Dis.* **12**, 452.
29. Patel, A., Lee, H.O., Jawerth, L., Maharana, S., Jahnel, M., Hein, M.Y., Stoynov, S., Mahamid, J., et al., (2015). A Liquid-to-Solid Phase Transition of the ALS Protein FUS Accelerated by Disease Mutation. *Cell* **162**, 1066–1077.
30. Molliex, A., Temirov, J., Lee, J., Coughlin, M., Kanagaraj, A.P., Kim, H.J., Mittag, T., Taylor, J.P., (2015). Phase separation by low complexity domains promotes stress granule assembly and drives pathological fibrillization. *Cell* **163**, 123–133.
31. Alberti, S., Gladfelter, A., Mittag, T., (2019). Considerations and Challenges in Studying Liquid-Liquid Phase Separation and Biomolecular Condensates. *Cell* **176**, 419–434.
32. Amini, F., Kodadek, T., Brown, K.C., (2002). Protein affinity labeling mediated by genetically encoded peptide tags. *Angew. Chem. Int. Ed. Engl.* **41**, 356–359.
33. Rhee, H.W., Zou, P., Udeshi, N.D., Martell, J.D., Mootha, V.K., Carr, S.A., Ting, A.Y., (2013). Proteomic mapping of mitochondria in living cells via spatially restricted enzymatic tagging. *Science* **339**, 1328–1331.
34. Morelli, F.F., Mediani, L., Heldens, L., Bertacchini, J., Bigi, I., Carra, A.D., Vinet, J., Carra, S., (2017). An interaction study in mammalian cells demonstrates weak binding of HSPB2 to BAG3, which is regulated by HSPB3 and abrogated by HSPB8. *Cell Stress Chaperones* **22**, 531–540.
35. Huttlin, E.L., Bruckner, R.J., Navarrete-Perea, J., Cannon, J.R., Baltier, K., Gebreab, F., Gygi, M.P., Thornock, A., et al., (2021). Dual proteome-scale networks reveal cell-specific remodeling of the human interactome. *Cell* **184** 3022-3040 e3028.
36. Vos, M.J., Kanon, B., Kampinga, H.H., (2009). HSPB7 is a SC35 speckle resident small heat shock protein. *Biochim. Biophys. Acta* **1793**, 1343–1353.
37. Darling, A.L., Liu, Y., Oldfield, C.J., Uversky, V.N., (2018). Intrinsically Disordered Proteome of Human Membrane-Less Organelles. *Proteomics* **18**, e1700193.
38. Staby, L., O'Shea, C., Willemoes, M., Theisen, F., Kragelund, B.B., Skriver, K., (2017). Eukaryotic transcription factors: paradigms of protein intrinsic disorder. *Biochem. J* **474**, 2509–2532.
39. Liu, J., Perumal, N.B., Oldfield, C.J., Su, E.W., Uversky, V. N., Dunker, A.K., (2006). Intrinsic disorder in transcription factors. *Biochemistry* **45**, 6873–6888.
40. Sandhu, K.S., (2009). Intrinsic disorder explains diverse nuclear roles of chromatin remodeling proteins. *J. Mol. Recognit.* **22**, 1–8.
41. Dutagaci, B., Nawrocki, G., Goodluck, J., Ashkarran, A.A., Hoogstraten, C.G., Lapidus, L.J., Feig, M., (2021). Charge-driven condensation of RNA and proteins suggests broad role of phase separation in cytoplasmic environments. *Elife* **10**
42. Thul, P.J., Lindskog, C., (2018). The human protein atlas: A spatial map of the human proteome. *Protein Sci.* **27**, 233–244.
43. Clausen, T.H., Lamark, T., Isakson, P., Finley, K., Larsen, K.B., Brech, A., Overvatn, A., Stenmark, H., et al., (2010). p62/SQSTM1 and ALFY interact to facilitate the formation of p62 bodies/ALIS and their degradation by autophagy. *Autophagy* **6**, 330–344.
44. Ha, J.R., Hao, L., Venkateswaran, G., Huang, Y.H., Garcia, E., Persad, S., (2014). beta-catenin is O-GlcNAc glycosylated at Serine 23: implications for beta-catenin's subcellular localization and transactivator function. *Exp. Cell Res.* **321**, 153–166.
45. Sanbe, A., Osinska, H., Saffitz, J.E., Glabe, C.G., Kayed, R., Maloyan, A., Robbins, J., (2004). Desmin-related

cardiomyopathy in transgenic mice: a cardiac amyloidosis. *PNAS* **101**, 10132–10136.
46. Wang, X., Osinska, H., Klevitsky, R., Gerdes, A.M., Nieman, M., Lorenz, J., Hewett, T., Robbins, J., (2001). Expression of R120G-alphaB-crystallin causes aberrant desmin and alphaB-crystallin aggregation and cardiomyopathy in mice. *Circ. Res.* **89**, 84–91.
47. Hussein, R.M., Benjamin, I.J., Kampinga, H.H., (2015). Rescue of alphaB Crystallin (HSPB5) Mutants Associated Protein Aggregation by Co-Expression of HSPB5 Partners. *PLoS One* **10**, e0126761.
48. Kriehuber, T., Rattei, T., Weinmaier, T., Bepperling, A., Haslbeck, M., Buchner, J., (2010). Independent evolution of the core domain and its flanking sequences in small heat shock proteins. *FASEB J.* **24**, 3633–3642.
49. Haslbeck, M., Weinkauf, S., Buchner, J., (2019). Small heat shock proteins: Simplicity meets complexity. *J. Biol. Chem.* **294**, 2121–2132.
50. Geiger, T., Wehner, A., Schaab, C., Cox, J., Mann, M., (2012). Comparative proteomic analysis of eleven common cell lines reveals ubiquitous but varying expression of most proteins. *Mol. Cell. Proteomics* **11**
51. Srinivas, P.N., Reddy, P.Y., Reddy, G.B., (2008). Significance of alpha-crystallin heteropolymer with a 3:1 alphaA/alphaB ratio: chaperone-like activity, structure and hydrophobicity. *Biochem. J* **414**, 453–460.
52. Aquilina, J.A., Shrestha, S., Morris, A.M., Ecroyd, H., (2013). Structural and functional aspects of hetero-oligomers formed by the small heat shock proteins alphaB-crystallin and HSP27. *J. Biol. Chem.* **288**, 13602–13609.
53. Mymrikov, E.V., Daake, M., Richter, B., Haslbeck, M., Buchner, J., (2017). The chaperone activity and substrate spectrum of human small heat shock proteins. *J. Biol. Chem.* **292**, 672–684.
54. Minoia, M., Grit, C., Kampinga, H.H., (2014). HSPA1A-independent suppression of PARK2 C289G protein aggregation by human small heat shock proteins. *Mol. Cell Biol.* **34**, 3570–3578.
55. Prabhu, S., Raman, B., Ramakrishna, T., Rao Ch, M., (2012). HspB2/myotonic dystrophy protein kinase binding protein (MKBP) as a novel molecular chaperone: structural and functional aspects. *PLoS One* **7**, e29810.
56. Skouri-Panet, F., Michiel, M., Ferard, C., Duprat, E., Finet, S., (2012). Structural and functional specificity of small heat shock protein HspB1 and HspB4, two cellular partners of HspB5: role of the in vitro hetero-complex formation in chaperone activity. *Biochimie* **94**, 975–984.
57. Ferrolino, M.C., Mitrea, D.M., Michael, J.R., Kriwacki, R. W., (2018). Compositional adaptability in NPM1-SURF6 scaffolding networks enabled by dynamic switching of phase separation mechanisms. *Nat. Commun.* **9**, 5064.
58. Riback, J.A., Zhu, L., Ferrolino, M.C., Tolbert, M., Mitrea, D.M., Sanders, D.W., Wei, M.T., Kriwacki, R.W., et al., (2020). Composition-dependent thermodynamics of intracellular phase separation. *Nature* **581**, 209–214.
59. Christensen, N.R., Pedersen, C.P., Sereikaite, V., Pedersen, J.N., Vistrup-Parry, M., Sorensen, A.T., Otzen, D., Teilum, K., et al., (2022). Bidirectional protein-protein interactions control liquid-liquid phase separation of PSD-95 and its interaction partners. *iScience* **25**, 103808.
60. Alberti, S., Mateju, D., Mediani, L., Carra, S., (2017). Granulostasis: Protein Quality Control of RNP Granules. *Front. Mol. Neurosci.* **10**, 84.
61. den Engelsman, J., Bennink, E.J., Doerwald, L., Onnekink, C., Wunderink, L., Andley, U.P., Kato, K., de Jong, W.W., et al., (2004). Mimicking phosphorylation of the small heat-shock protein alphaB-crystallin recruits the F-box protein FBX4 to nuclear SC35 speckles. *Eur. J. Biochem.* **271**, 4195–4203.
62. Hyman, A.A., Weber, C.A., Julicher, F., (2014). Liquid-liquid phase separation in biology. *Annu. Rev. Cell Dev. Biol.* **30**, 39–58.
63. Shin, Y., Brangwynne, C.P., (2017). Liquid phase condensation in cell physiology and disease. *Science* **357**
64. Wignes, J.A., Goldman, J.W., Weihl, C.C., Bartley, M.G., Andley, U.P., (2013). p62 expression and autophagy in alphaB-crystallin R120G mutant knock-in mouse model of hereditary cataract. *Exp. Eye Res.* **115**, 263–273.
65. Bjorkoy, G., Lamark, T., Brech, A., Outzen, H., Perander, M., Overvatn, A., Stenmark, H., Johansen, T., (2005). p62/SQSTM1 forms protein aggregates degraded by autophagy and has a protective effect on huntingtin-induced cell death. *J. Cell Biol.* **171**, 603–614.
66. Settembre, C., Fraldi, A., Jahreiss, L., Spampanato, C., Venturi, C., Medina, D., de Pablo, R., Tacchetti, C., et al., (2008). A block of autophagy in lysosomal storage disorders. *Hum. Mol. Genet.* **17**, 119–129.
67. Boncoraglio, A., Minoia, M., Carra, S., (2012). The family of mammalian small heat shock proteins (HSPBs): implications in protein deposit diseases and motor neuropathies. *Int. J. Biochem. Cell Biol.* **44**, 1657–1669.
68. Erdos, G., Pajkos, M., Dosztanyi, Z., (2021). IUPred3: prediction of protein disorder enhanced with unambiguous experimental annotation and visualization of evolutionary conservation. *Nucleic Acids Res.* **49**, W297–W303.
69. Vincent, M., Schnell, S., (2019). Disorder Atlas: Web-based software for the proteome-based interpretation of intrinsic disorder predictions. *Comput. Biol. Chem.* **83**, 107090.
70. Vincent, M., Schnell, S., (2016). A collection of intrinsic disorder characterizations from eukaryotic proteomes. *Sci. Data* **3**, 160045.
71. Dosztanyi, Z., Csizmok, V., Tompa, P., Simon, I., (2005). The pairwise energy content estimated from amino acid composition discriminates between folded and intrinsically unstructured proteins. *J. Mol. Biol.* **347**, 827–839.
72. Dosztanyi, Z., Csizmok, V., Tompa, P., Simon, I., (2005). IUPred: web server for the prediction of intrinsically unstructured regions of proteins based on estimated energy content. *Bioinformatics* **21**, 3433–3434.
73. Kozlowski, L.P., (2017). Proteome-pI: proteome isoelectric point database. *Nucleic Acids Res.* **45**, D1112–D1116.
74. Kubitz, L., Bitsch, S., Zhao, X., Schmitt, K., Deweid, L., Roehrig, A., Barazzone, E.C., Valerius, O., et al., (2022). Engineering of ultraID, a compact and hyperactive enzyme for proximity-dependent biotinylation in living cells. *Commun. Biol.* **5**, 657.
75. Verschuure, P., Tatard, C., Boelens, W.C., Grongnet, J.F., David, J.C., (2003). Expression of small heat shock proteins HspB2, HspB8, Hsp20 and cvHsp in different tissues of the perinatal developing pig. *Eur. J. Cell Biol.* **82**, 523–530.
76. Wilhelmus, M.M., Otte-Holler, I., Wesseling, P., de Waal, R.M., Boelens, W.C., Verbeek, M.M., (2006). Specific association of small heat shock proteins with the pathological hallmarks of Alzheimer's disease brains. *Neuropathol. Appl. Neurobiol.* **32**, 119–130.

77. O'Connor, S.J., Forsyth, P.D., Dalal, S., Evans, P.A., Short, M.A., Shiach, C., Jack, A.S., Morgan, G.J., (1997). The rapid diagnosis of acute promyelocytic leukaemia using PML (5E10) monoclonal antibody. *Br. J. Haematol.* **99**, 597–604.
78. Schindelin, J., Arganda-Carreras, I., Frise, E., Kaynig, V., Longair, M., Pietzsch, T., Preibisch, S., Rueden, C., et al., (2012). Fiji: an open-source platform for biological-image analysis. *Nat. Methods* **9**, 676–682.
79. van der Walt, S., Schonberger, J.L., Nunez-Iglesias, J., Boulogne, F., Warner, J.D., Yager, N., Gouillart, E., Yu, T., et al., (2014). Scikit-image: image processing in Python. *PeerJ* **2**, e453.
80. Virtanen, P., Gommers, R., Oliphant, T.E., Haberland, M., Reddy, T., Cournapeau, D., Burovski, E., Peterson, P., et al., (2020). SciPy 1.0: fundamental algorithms for scientific computing in Python. *Nat. Methods* **17**, 261–272.
81. Rappsilber, J., Mann, M., Ishihama, Y., (2007). Protocol for micro-purification, enrichment, pre-fractionation and storage of peptides for proteomics using StageTips. *Nat. Protoc.* **2**, 1896–1906.
82. Cox, J., Mann, M., (2008). MaxQuant enables high peptide identification rates, individualized p.p.b.-range mass accuracies and proteome-wide protein quantification. *Nat. Biotechnol.* **26**, 1367–1372.
83. Perez-Riverol, Y., Csordas, A., Bai, J., Bernal-Llinares, M., Hewapathirana, S., Kundu, D.J., Inuganti, A., Griss, J., et al., (2019). The PRIDE database and related tools and resources in 2019: improving support for quantification data. *Nucleic Acids Res.* **47**, D442–D450.
84. Tyanova, S., Temu, T., Sinitcyn, P., Carlson, A., Hein, M. Y., Geiger, T., Mann, M., Cox, J., (2016). The Perseus computational platform for comprehensive analysis of (prote)omics data. *Nat. Methods* **13**, 731–740.
85. Ashburner, M., Ball, C.A., Blake, J.A., Botstein, D., Butler, H., Cherry, J.M., Davis, A.P., Dolinski, K., et al., (2000). Gene ontology: tool for the unification of biology. The Gene Ontology Consortium. *Nat. Genet.* **25**, 25–29.
86. Gene Ontology, C., (2021). The Gene Ontology resource: enriching a GOld mine. *Nucleic Acids Res.* **49**, D325–D334.
87. Mi, H., Muruganujan, A., Ebert, D., Huang, X., Thomas, P. D., (2019). PANTHER version 14: more genomes, a new PANTHER GO-slim and improvements in enrichment analysis tools. *Nucleic Acids Res.* **47**, D419–D426.